iScience

Article

Complement is primarily activated in the lung in a mouse model of severe COVID-19

Graphical abstract

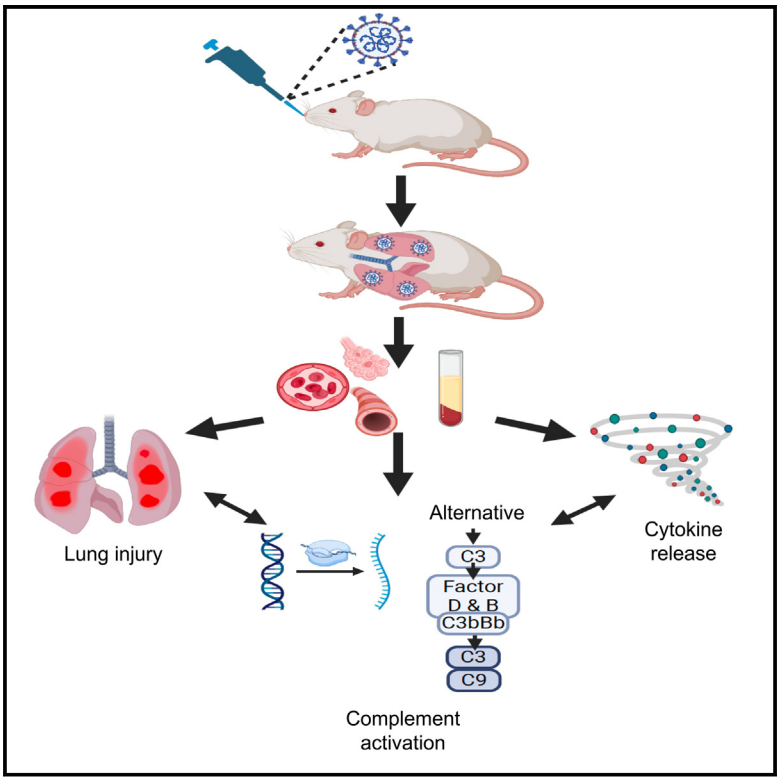

Authors

Peter J. Szachowicz, Christine Wohlford-Lenane, Cobey J. Donelson, ..., Yuzhou Zhang, Richard J.H. Smith, Paul B. McCray, Jr.

Correspondence

peter-szachowicz@uiowa.edu (P.J.S.), paul-mccray@uiowa.edu (P.B.M.)

In brief

Respiratory medicine; Immunology

Highlights

- SARS-CoV-2 infected mice have increased lung and serum complement biomarkers
- Post-infection, pulmonary complement deposits in the airways, alveoli, and blood vessels
- Respiratory epithelia increase complement gene transcription post-SARS-CoV-2 infection
- Describes an animal model to study complement inhibitors for COVID-19 treatment

Szachowicz et al., 2025, iScience *28*, 111930
March 21, 2025 Published by Elsevier Inc.
https://doi.org/10.1016/j.isci.2025.111930

CellPress

iScience

CellPress
OPEN ACCESS

Article

Complement is primarily activated in the lung in a mouse model of severe COVID-19

Peter J. Szachowicz,[1,7,*] Christine Wohlford-Lenane,[2] Cobey J. Donelson,[3] Shreya Ghimire,[1] Andrew Thurman,[1] Biyun Xue,[2] Timothy J. Boly,[2] Abhishek Verma,[5] Leila MašinoviĆ,[1] Jennifer R. Bermick,[2] Tayyab Rehman,[6] Stanley Perlman,[2,5] David K. Meyerholz,[4] Alejandro A. Pezzulo,[1] Yuzhou Zhang,[3] Richard J.H. Smith,[3] and Paul B. McCray, Jr.[2,5,*]

[1]Department of Internal Medicine, The University of Iowa, Division of Pulmonary, Critical Care, and Occupational Medicine, Iowa City, IA 52242, USA
[2]Stead Family Department of Pediatrics, The University of Iowa, Iowa City, IA 52242, USA
[3]Molecular Otolaryngology and Renal Research Laboratories, Carver College of Medicine, University of Iowa, Iowa City, IA, USA
[4]Department of Pathology, The University of Iowa, Iowa City, IA 52242, USA
[5]Department of Microbiology and Immunology, The University of Iowa, Iowa City, IA 52242, USA
[6]Department of Inernal Medicine, University of Michigan, Division of Pulmonary and Critical Care Medicine, Ann Arbor, MI 48109, USA
[7]Lead contact
*Correspondence: peter-szachowicz@uiowa.edu (P.J.S.), paul-mccray@uiowa.edu (P.B.M.)
https://doi.org/10.1016/j.isci.2025.111930

SUMMARY

In vitro studies and observational human disease data suggest the complement system contributes to SARS-CoV-2 pathogenesis, although how complement dysregulation develops in severe COVID-19 is unknown. Here, using a mouse-adapted SARS-CoV-2 virus (SARS2-N501Y_{MA30}) and a mouse model of COVID-19, we identify significant serologic and pulmonary complement activation post-infection. We observed C3 activation in airway and alveolar epithelia, and pulmonary vascular endothelia. Our evidence suggests the alternative pathway is the primary route of complement activation, however, components of both the alternative and classical pathways are produced locally by respiratory epithelial cells following infection, and increased in primary cultures of human airway epithelia following cytokine and SARS-CoV-2 exposure. This tissue-specific complement response appears to precede lung injury and inflammation. Our results suggest that complement activation is a defining feature of severe COVID-19 in mice, agreeing with previous publications, and provide the basis for further investigation into the role of complement in COVID-19.

INTRODUCTION

The COVID-19 pandemic has resulted in >7 million deaths worldwide (https://covid19.who.int/). Through a global scientific effort, we have learned much about SARS-CoV-2 and COVID-19 pathophysiology. COVID-19 exists on a spectrum from mild disease, characterized by minimal vague and generalized symptoms, to severe illness, with the most critically ill suffering from a combination of acute respiratory distress syndrome (ARDS) and multi-organ failure.[1] Although the advent of effective vaccines and antiviral treatments has reduced hospitalizations and death,[2–7] treatment for patients presenting with respiratory failure remains ineffective.[5–7] With the ongoing threat of virulent mutations and pathogenic variants,[8,9] research that improves our understanding of this disease and identifies novel therapeutic options remains critical.

Reported pathophysiologic features of severe COVID-19 include prothrombotic complications,[10–13] "cytokine storm,"[14,15] NETosis,[16] and excessive cytotoxic T cell responses,[17] all of which can be driven by complement activation.[18] Complement is an ancient and evolutionarily conserved arm of the immune system.[19,20] The role of complement is most classically considered in the context of innate immunity; however, its function as a mediator of the adaptive immune response (both cell mediated and humoral) is well established.[20–23] Additionally, several non-canonical functions of complement have been identified including roles in cell metabolism, autophagy, and apoptosis.[24–26] While most commonly understood as liver-derived proteins, some cell types produce complement proteins locally,[27,28] with the lungs representing a large reservoir of extrahepatic complement production.[29] In the context of infections, complement is a key mediator of the host response to respiratory viruses, including other pathologic human coronaviruses.[30–32] In particular, SARS-CoV-2 is associated with complement dysregulation locally and systemically. Genomic and proteomic studies have confirmed autopsy results demonstrating COVID-19 patients have an increased complement response compared to ARDS from other causes, and patients with underlying disorders characterized by complement overactivation are prone to developing more severe disease than matched cohorts.[33–36] Thus, evidence supports the idea that SARS-CoV-2 infection may activate complement and this may contribute to disease severity.

Despite evidence for complement involvement in COVID-19, significant gaps remain in our understanding of its contributions to this disease. For example, there is no consensus on which complement pathway is primarily activated. In patients hospitalized with severe COVID-19, data from serum and lung bronchoalvoler lavage fluid samples suggest an increase in complement proteins associated with the alternative pathway (AP) is a consistent feature of severe disease, and is associated with worse prognosis.[34,37] Interestingly, activation of the classical pathway (CP) and lectin pathway (LP) has also been demonstrated in such patients by proteomics studies and direct measurement of complement biomarkers,[35,38,39] with histopathologic evidence from autopsies also confirming deposition of LP-specific proteins (i.e., MASP-2) within the lungs. *In vitro* data also support that complement proteins specific to all three complement pathways (i.e., mannose binding lectin [MBL] of the LP, factor D and pentraxin 3 of the AP, and C1q of the CP) can bind to SARS-CoV-2 structural proteins[40–44] and subsequently activate their respective complement cascades. Overall, the question of whether a specific complement pathway is primarily activated in severe COVID-19 and drives the observed inflammatory response is unanswered, and deserves further investigation, as this has important mechanistic implications and could inform effective treatment strategies for this disease. Likewise, whether SARS-CoV-2 antigens activate complement directly or indirectly by stimulating inflammatory and immune mediators remains uncertain.[40,42,43] Respiratory epithelial cells do generate complement in response to cell injury and inflammation[45,46] and this response has been demonstrated in cultured primary human alveolar type II cells following SARS-CoV-2 infection.[43] However, confirmatory human and animal model data are lacking, and therefore, the impact of complement on COVID-19 disease pathogenesis remains undefined.

To address this knowledge gap, we investigated the role of complement in a mouse model of COVID-19 that recapitulates many features of severe disease in humans. We demonstrate that following infection, complement activation is detected in both serum and lungs as early as 2 days post-infection (dpi). This complement activation occurs primarily via the AP and is specific to the lungs, with mice developing an extensive complement burden with terminal complement cascade (TCC) activation. We found C3 co-localization in alveoli, airways, and blood vessels suggesting activation on these cell surfaces. Importantly, we also show complement deposition is not strictly limited to infected respiratory epithelial cells, suggesting complement activation extends beyond direct antiviral mechanisms. This study provides the first demonstration in an animal model of severe COVID-19 that complement protein C3 is locally produced and activated in the lung where it may play a direct role in disease pathogenesis.

RESULTS

SARS2-N501Y$_{MA30}$ reproduces the clinical phenotype of severe COVID-19

We previously reported the development of a COVID-19 mouse model that recapitulates features of severe disease comparable to what is observed in hospitalized human patients with respiratory failure due to viral pneumonia and associated acute lung injury.[47] To investigate the complement response, we infected young (6–8 week old) BALB/c mice intranasally with 5,000 plaque-forming unit (PFU) of SARS2-N501Y$_{MA30}$ virus, and euthanized mice on 0–5 dpi for sample collection. A second group was monitored for weight loss and mortality (Figure 1A; Figures S1A and S1B). All virus-treated mice succumbed to infection by 7 dpi (Figure 1B) and lost ~30% of their body weight (Figure 1C). Interestingly, we observed a sex specific response to infection and noted a trend toward improved survival for females (Figure S2), consistent with other murine models of SARS-CoV-2 infection.[48] In evaluating respiratory viral burden, we saw peak SARS2-N501Y$_{MA30}$ nucleocapsid protein (N-protein) antigen staining by 2 dpi, with evidence of viral clearance by 4 dpi (Figures 1D and 1E); a pattern confirmed with viral titer by plaque assay (Figure 1F). In all, the mice met metrics indicative of severe disease.

Complement response following infection with SARS2-N501Y$_{MA30}$

We hypothesized that, like humans with COVID-19, mice infected with SARS2-N501Y$_{MA30}$ would mount a complement response in the lungs. To test this hypothesis, lung homogenates were collected from infected mice at 2 and 4 dpi, which correspond with the peak viral burden (Figures 1D–1F) and peak illness severity before death (Figures 1B and 1C), respectively. To evaluate the degree of complement cascade protein deposition (Figure 2), we quantified factor B (FB) (AP specific), C3 (common cascade), and C4 (CP and LP specific) proteins in lung tissue (Figure 3). Pulmonary iC3b and C3d were elevated at 4 dpi on both western blot (Figure 3A) and C3/C3b by ELISA (Figures 3D and 3E), suggesting C3 convertase is formed in lung tissue with substantial C3 cleavage product formation. AP specific FB and Bb were also significantly elevated on 4 dpi (Figure 3B). While we detected C4 (Figure 3C), it was not significantly increased compared to controls. Data for 2 dpi demonstrate a similar pattern, suggesting C3 and FB deposition post-infection, with no significant change in lung C4 levels (Figure S3). We evaluated TCC activity in the lungs following SARS2-N501Y$_{MA30}$ infection using C9 levels as a surrogate for downstream complement cascade activity, and demonstrated increased C9 protein by immunoblot and immunofluorescence staining at 4 dpi (Figures 4A and 4B), as well as increased serologic activation and consumption of AP specific complement components as indicated by decreased alternative pathway functional assay (APFA) activity on 4 dpi (Figure 4C). C9 deposition in the lungs was primarily detected along the airways, interalveolar septa, and blood vessels, consistent with autopsy descriptions from human patients[49] (Figure S4). Of note, we observed no consistent differences between male and female mice on western blot, though the C3b ELISA showed a trend toward increased levels in males on 2 and 4 dpi.

We hypothesized that C3 would co-localize to cells infected with SARS2-N501Y$_{MA30}$. To test this hypothesis, we immunolocalized the viral N-protein and C3 in infected tissues and observed that while C3 co-localized with N-protein at 2 and 4 dpi, C3 also deposited in cells with no detectable N-protein (Figure 5A; Figure S6A), suggesting a potential indirect mechanism of C3 activation.

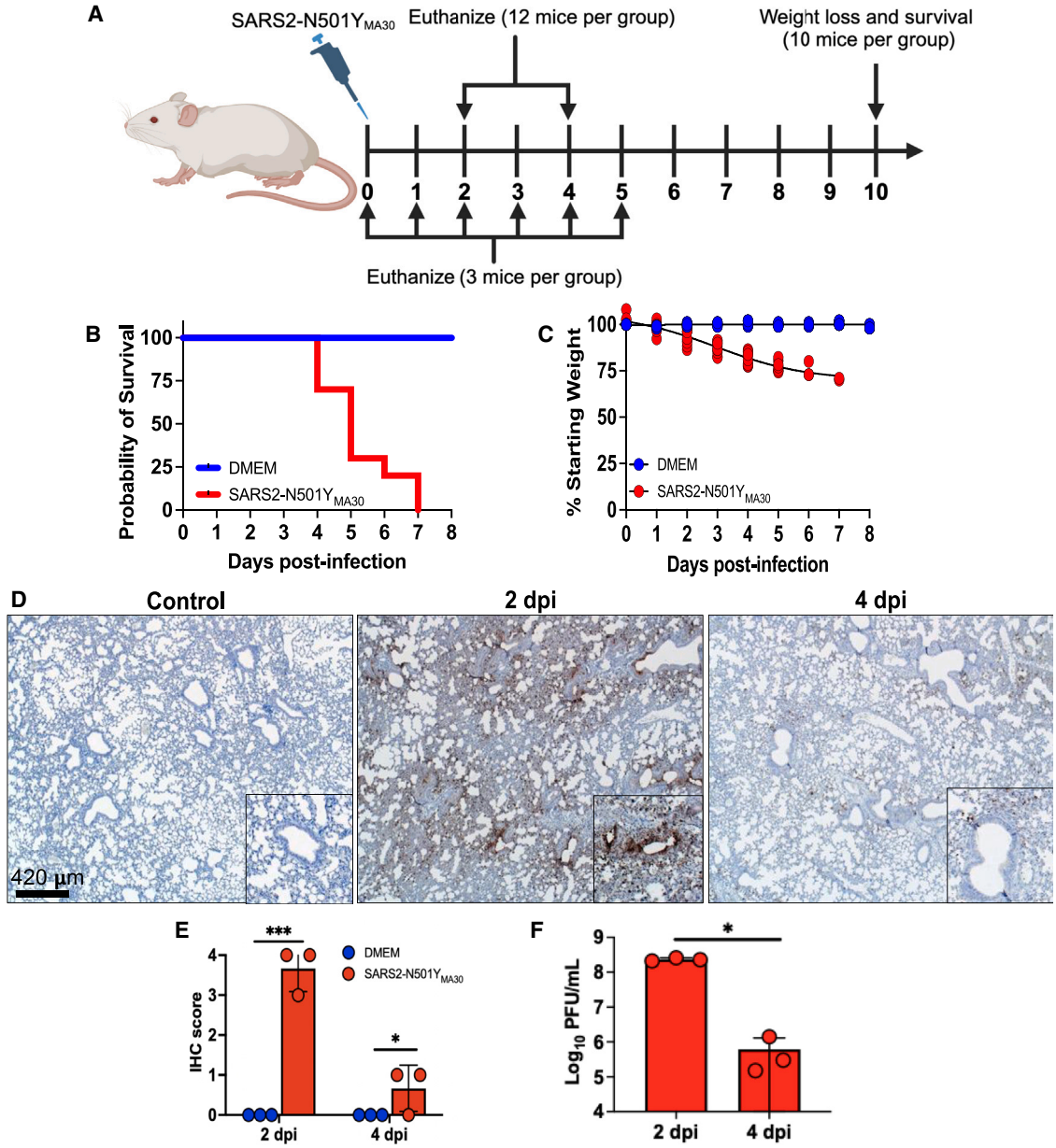

Figure 1. BALB/c mice infected with SARS2-N501Y$_{MA30}$ develop severe disease with peak respiratory viral burden 2 dpi

(A) Schematic of the experimental protocol in which mice were inoculated with 5,000 PFU of SARS2-N501Y$_{MA30}$ and either euthanized or monitored. Groups contained even numbers of males and females.

(B) Probability of survival following SARS2-N501Y$_{MA30}$ infection (red) compared to control group (blue) with significance achieved by 5 dpi, $p < 0.05$.

(C) Mean ± SEM weight loss post-infection assessed by percent decrease from initial weight at each time point with significant difference achieved by 3 dpi, $p < 0.05$ ($n = 10$ mice per group).

(D) Immunohistochemical (IHC) staining for SARS2-N501Y$_{MA30}$ nucleocapsid protein (N-protein) (brown = N protein, $n = 3$ mice) at 2 dpi with significant involvement of alveoli, airways, and perivascular infiltrates. At 4 dpi, there is a similar pattern of viral burden, though N-protein deposition is less dense. Representative insets are included.

(E and F) (E) IHC scoring for severity by percent area of lung stained positive for viral antigen and (F) viral titer obtained from plaque assay of lung tissue homogenates ($n = 3$ mice). Red = SARS2-N501Y$_{MA30}$ and blue = DMEM (significance determined by log rank test and unpaired t test, where * indicates $p < 0.05$ and *** indicates $p < 0.001$). DMEM, Dulbecco's modified Eagle's medium. Error bars represent mean ± SEM.

To identify the cell types responsible for pulmonary C3 activation, we immunolocalized C3 in lung tissue sections. C3 deposition was notable as early as 1 dpi (Figure S5), with extensive involvement by 4 dpi (Figure 5B). C3 expression was diffuse, with localization to airways, alveoli, and blood vessels. Of note, these regions of the lung are common sites of injury in

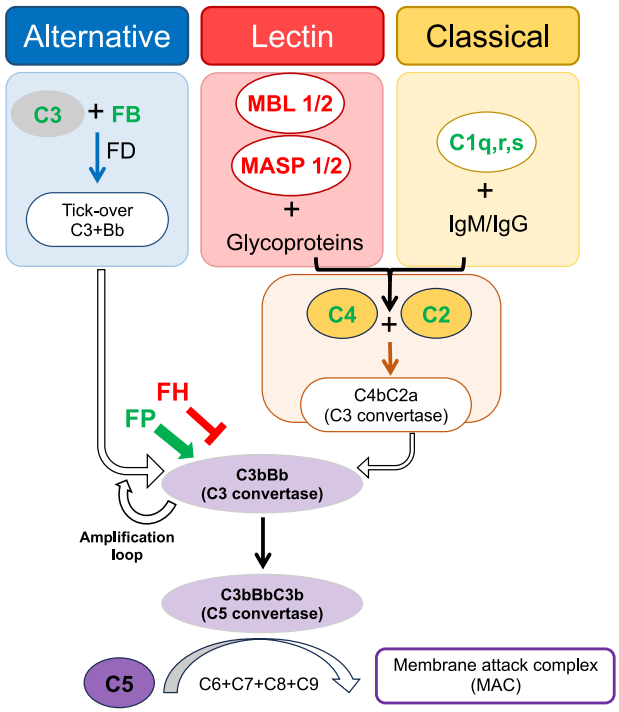

Figure 2. Schematic of complement cascade and components up-regulated by SARS-CoV-2 infection

Green text indicates proteins with increased mRNA transcripts in mice following SARS2-N501Y$_{MA30}$ infection, red text indicates proteins with reduced mRNA transcript abundance in mice following SARS2-N501Y$_{MA30}$ infection. As depicted, the alternative pathway is continuously and spontaneously activated at low levels (tick-over) to generate C3bBb (C3 convertase), though rapid self-enhancement occurs by feedback amplification loop once activation is initiated. The lectin and classical pathways have different triggering substrates (glycoproteins and immunoglobulins, respectively), but both converge on the generation of C4 and C2, which join to create the C3 convertase C4bC2a. Although the lectin and classical pathways are initiated via separate mechanisms, a majority of their activity ultimately converges on C3bBb (C3 convertase), which cleaves C3 into C3a (anaphylatoxin) and C3b (opsonin). All three pathways coalesce with C5 convertase cleavage of C5, and the generation of C5a (anaphylatoxin) and C5b (joins with C6-C9 to form C5b-9, membrane attack complex). In addition, there are various cofactor proteins that help regulate cascade activity, such as properdin (FP) and complement factor H (FH), which can augment or inhibit further activation, respectively. FB, factor B; MBL, mannose binding lectin; MASP, MBL-associated serine protease; FD, factor D.

COVID-19 patients with small airways disease, diffuse alveolar damage, and pulmonary vascular thrombosis.[50,51] We further characterized this C3 deposition in the lung tissue finding C3 localized to cells at lumenal surfaces (Figures 5B and 5C; Figure S6B). By co-staining for C3 and HopE-1 (type I alveolar cell marker), acetylated α-tubulin (ciliated cell marker), and von Willebrand factor (vWF, endothelial cell marker), we found C3 co-localized with these cell types along their apical membranes (Figures 5C–5E; Figures S6C–S6E), confirming C3 associates with cell types in multiple sub-compartments in the lungs, including those where little or no viral infection occurred (Figure 5A). We observed a similar distribution of C9 on IF staining (Figure 4B). The apical polarization of C3 and C9 also suggests the presence of membrane-bound convertase and membrane attack complex (MAC) formation on the lumenal cell surface. Of note, we also localized C4 in the lungs of infected mice, but expression did not change substantially over the course of infection, consistent with immunoblot data.

These results are consistent with extensive C3 and C9 activity in the lung following SARS2-N501Y$_{MA30}$ infection, and suggest C3 convertase formation by activation by the AP in the absence of any significant change in CP or LP activity.

Local complement gene transcription by respiratory epithelial cells

Although the observed pulmonary C3 could be explained by deposition of circulating complement, we suspected an alternate etiology. Extrahepatic complement production by respiratory epithelial cells has been described[52] and given the abundance of complement detected in lung tissue, we hypothesized respiratory epithelial cells were sources of local production. To that end, we performed RNAscope for C3 and found RNA transcripts in respiratory epithelial cells in mice infected with SARS2-N501Y$_{MA30}$ (Figure 6A). C3 and SARS2-N501Y$_{MA30}$ RNA transcripts colocalized at 2 dpi (Figures 6A; Figure S7), confirming that infected cells express C3. However, C3 mRNA was also observed in SARS2-N501Y$_{MA30}$-negative cells consistent with the aforementioned findings that uninfected cells are also sources for C3 in the lungs. We hypothesized these uninfected cells were generating complement in response to cytokines released by neighboring cells and binding their respective receptors. Respiratory epithelial cells produce interleukin (IL)-17 and transforming growth factor α (TNF-α) in response to various respiratory viral infections including SARS-CoV-2,[53–57] and these cytokines, among others (i.e., IL-1β and IL-6), can induce complement synthesis.[58,59] This suggested the hypothesis that a paracrine or systemic cytokine response may trigger production of C3 by respiratory epithelial cells. Thus, we exposed primary cultures of human airway epithelia (HAE) to a cocktail of IL-17 and TNF-α and demonstrated the upregulation of C3 mRNA and numerous genes involved in the complement cascade, further supporting this as a mechanism that might explain our findings (Figure S8).

To evaluate whether mice infected with SARS2-N501Y$_{MA30}$ also had evidence increased transcription of complement genes other than C3, we performed bulk RNA sequencing (RNA-seq) of infected mouse lung tissue at 5 dpi. This showed increased expression of complement cascade mRNA transcripts compared with control animals (Figure 6B). Based on fold change, we observed significant increases in expression of *Cfb* (complement FB) and *Cfp* (complement factor properdin) post-infection, both specific to the AP (Figure 6C). Contrary to protein analyses, both CP and AP RNA transcripts were increased. We observed decreased expression of *Masp2 and Mbl1*, which are LP specific genes, as well as a decrease in *Cfh* (complement factor H) transcripts, a major regulator of complement activity. Of note, there was a large increase in *C3ar1* gene expression. C3aR is a receptor for the anaphylatoxin C3a, and its stimulation can result in the release of cytokines from epithelial and immune cells.

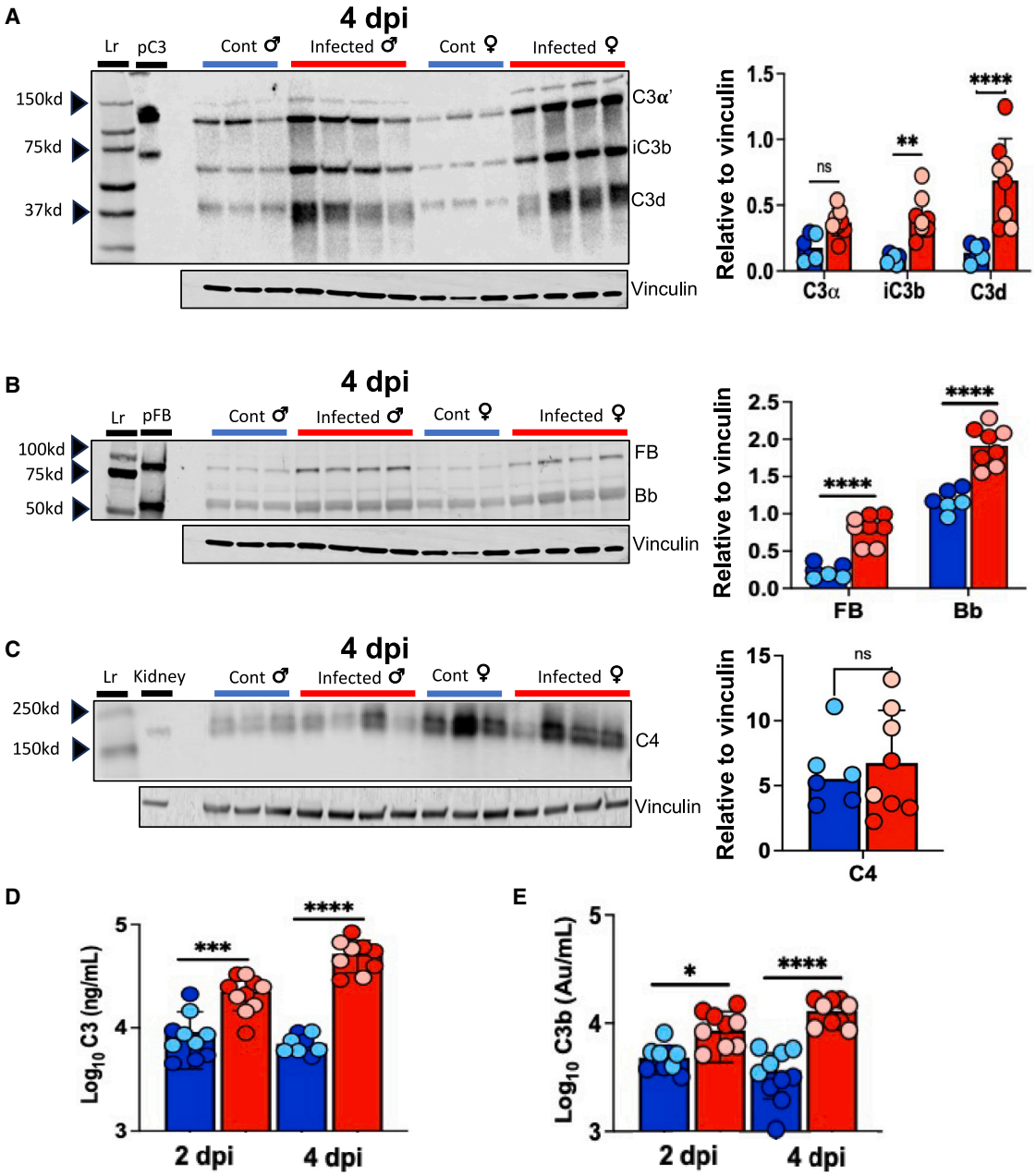

Figure 3. Increased C3 and FB activation in lungs of mice infected with SARS2-N501Y$_{MA30}$

(A–C) Western blot of lung homogenates with corresponding densitometry (right) demonstrates increases in iC3b and C3d (A) and FB and Bb (B), but not C4 (C) on 4 dpi. Purified human C3 (pC3), purified FB and Bb (pFB), and uninfected mouse kidney homogenates were used as controls for C3, FB, and C4, respectively. (D and E) ELISA for C3 and C3b of lung tissue homogenates demonstrates increases with SARS2-N501Y$_{MA30}$ infection compared to control lung at 2 and 4 dpi. Blue bars indicate samples from control mice, red bars indicate samples from infected mice, light blue and light red circles indicate females, dark blue and dark red circles indicate males. n = 10 mice per group. Significance as determined by one-way ANOVA and unpaired t test, $^{*}p < 0.05$,$^{**}p < 0.01$, $^{***}p < 0.001$, $^{****}p < 0.0001$. Lr, ladder. Error bars represent mean ± SEM.

In summation, these findings suggest infection stimulates a widespread complement response that is driven by locally derived complement proteins. Both overactivation and impaired regulation of the AP contribute to a dysregulated complement response in animals following SARS2-N501Y$_{MA30}$ infection.

Systemic complement response following SARS2-N501Y$_{MA30}$ infection

To evaluate whether systemic complement activity increases post-infection, we collected serum at 2 and 4 dpi and measured complement proteins by ELISA. Serum C3 levels in infected mice were increased compared to controls (Figure 7A), as was serum

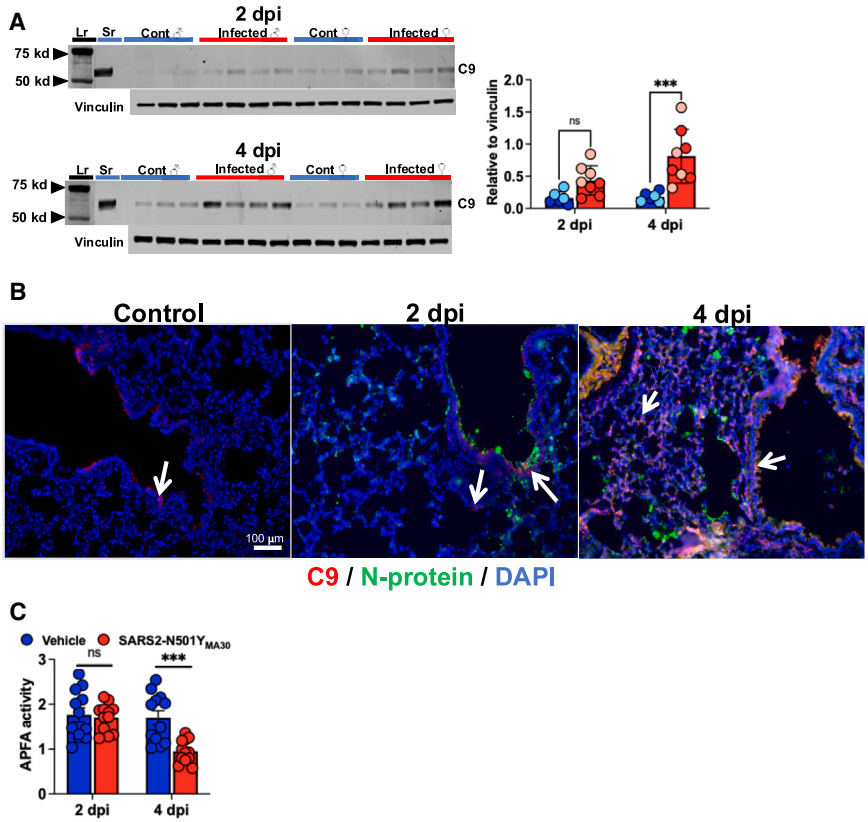

Figure 4. Evidence of increased complement C9 and alternative pathway activity in the serum and lungs post-SARS2-N501Y$_{MA30}$ infection

(A) Western blot for complement C9 protein in lung tissue homogenates shows increased levels at 4 dpi. (significance determined by one-way ANOVA where $^{***}p < 0.001$).

(B) Immunofluorescence staining for C9 (red) shows increased deposition within the alveoli and airways of the lungs at 4 dpi (white arrows indicate areas of C9 deposition). SARS2-N501Y$_{MA30}$ N-protein (green) suggests some areas of co-staining with C9.

(C) Serum alternative pathway functional assay (APFA) comparing control (blue) and SARS2-N501Y$_{MA30}$ (red) infected mice demonstrates similar activity levels on 2 dpi, with decreased activity in infected mice at 4 dpi, indicative of excess activation and consumption of alternative pathway specific complement proteins ($^{***}p < 0.001$), $n = 10$ mice per group. Blue bars represent control, red bars indicate SARS2-N501Y$_{MA30}$ infected mice, light blue and red circles indicate females, dark blue and red circles indicate males. Sr, mouse serum at 1:20 dilution for control; Lr, ladder. Error bars represent mean ± SEM.

C4 (Figure 7B). CH_{50}, used to assess classical and terminal complement pathway activity, was increased at 2 dpi but fell to control levels at 4 dpi (Figure 7C). Immunoblot for C3 protein on kidney homogenate of infected mice (Figure S9) showed no increase in C3 deposition, indicating the observed C3 response was limited to the lung. These findings suggest a concommitent increase in systemic complement following SARS2-N501Y$_{MA30}$ infection, with activity primarily involving the lung.

As stated previously, male mice had a more severe disease phenotype, a finding also described in human COVID-19 patients,[60] prompting us to question whether there were sex differences in systemic complement responses to SARS2-N501Y$_{MA30}$. Infected male mice had significantly increased serum C3 and CH_{50} activity compared to females (Figures 7D and 7F). Importantly, C4 expression post-infection was not significantly different between sexes (Figure 7E), indicating the observed difference in sex-specific complement activity is primarily via increased AP complement activation in response to SARS2-N501Y$_{MA30}$ infection that correlated to trends observed in the lungs.

Complement response may contribute to lung pathology and inflammatory response

When evaluating the pattern of lung injury (Figure 8A; Figure S10), we noted that mice develop evidence of lung injury on 2 dpi, which further advances by 4 dpi, whereas mice develop a significant complement response by 1 dpi (Figure S5), followed by a substantial cytokine response by 2 dpi (Figure 8B). There is subsequent limited immune cell infiltration on 2 dpi that becomes significant and widespread by 4 dpi[47] (Figure S10). Complement components C3a and C5a are potent anaphylatoxins.[61] To investigate the cytokine-chemokine profile in the setting of complement activation, we quantified concentrations of chemokines and cytokines in serum and lung homogenates at 0 to 5 dpi (Figure 8B). RANTES (CCL5), IL-1β, IL-6, CXCL-1, MCP-1, and CXCL-10 were elevated with infection, cytokines that have been associated with C3aR and C5aR1 stimulation.[62–65] We assessed mouse lung inflammatory gene expression from the bulk RNA-seq data at 5 dpi (Figure S11) and found increased transcription of genes associated with interferon signaling, as well as those typical of NLRP3 inflammasome and Toll-like receptor (TLR) mediated inflammation.

DISCUSSION

This study provides the first in-depth description of complement activity in an animal model of severe COVID-19. Our observations offer insights into an important aspect of this disease, with potential implications for other infectious and non-infectious forms of acute lung injury. Key findings include the following: (1) in response to SARS2-N501Y$_{MA30}$ infection, complement activity is significantly increased in the lung (locally) and circulation (systemically); (2) this activity is in part locally derived from respiratory epithelial cells; (3) complement activation occurs primarily through the AP; (4) complement production and activation by respiratory epithelial cells is not limited to virus infected cells; (5) complement may contribute to the observed COVID-19 pathophysiology by causing lung injury and inflammation.

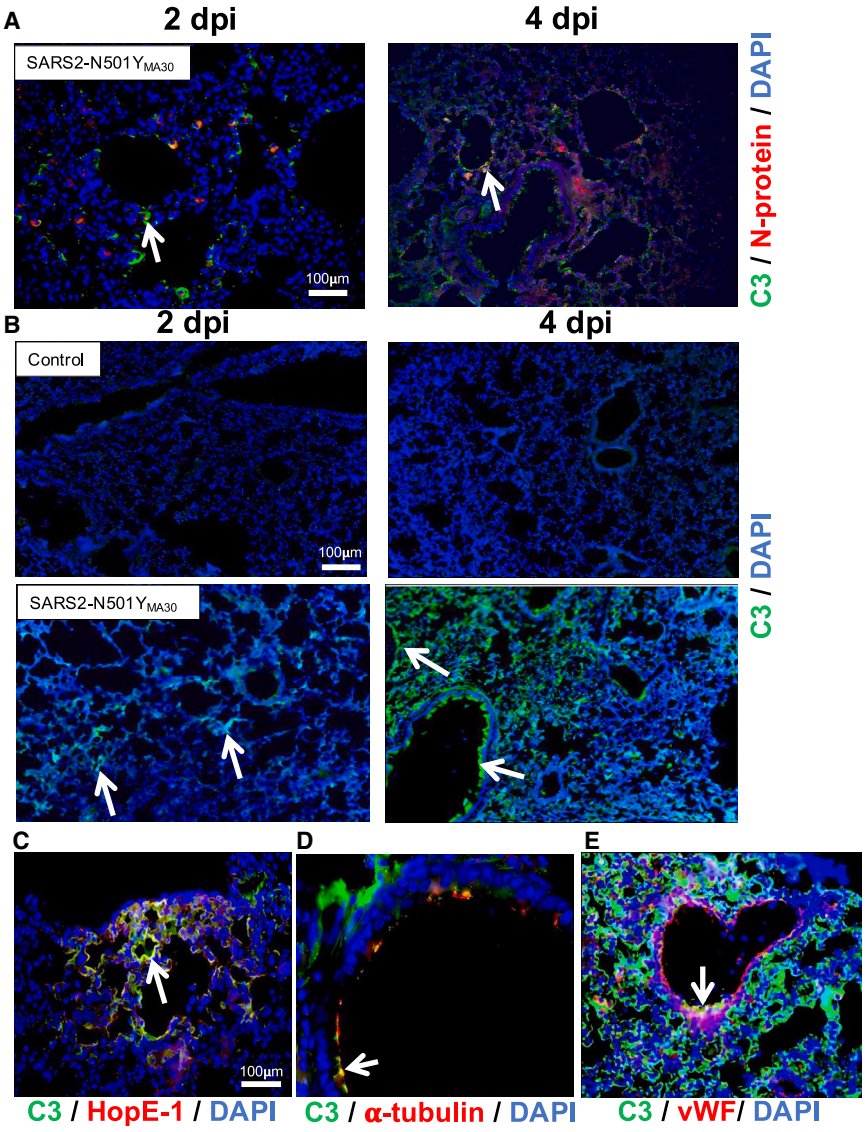

Figure 5. Complement C3 is colocalized with cells in various pulmonary sub compartments

(A) Colocalization of C3 (green) and SARS2-N501Y$_{MA30}$ nucleocapsid protein (red) on 2 and 4 dpi. *n* = 5, blue = DAPI, red = nucleocapsid protein, green = C3, white arrows indicate areas with C3 and nucleocapsid protein colocalization.

(B) Staining for complement C3 in lung tissue from control (top row) and following infection with SARS2-N501Y$_{MA30}$ (bottom row) on 2 and 4 dpi. White arrows indicate areas of C3 staining. *n* = 5, green = C3, blue = DAPI.

(C–E) (C) Colocalization of C3 with alveolar type I cells, (D) ciliated airway cells, and (E) endothelial cells on 4 dpi. White arrows indicate regions of colocalization with C3. dpi, days post-infection; vWF, von Willebrand factor.

Early in the course of infection, we observed significant C3 deposition in the lung, which becomes more diffuse by 4 dpi. The C3 and C9 protein is apically polarized and involves lumenal membranes of cells. C3 colocalizes with cells specific to airways, alveoli, and blood vessels. These cells form the subcompartments of the lung that are primary areas of injury in COVID-19 ARDS. The detection of significant C3b levels shows that C3 convertase is formed and the complement cascade is active, and the increased pulmonary C9 with a similar distribution pattern in the lung as C3 suggests C5-convertase activity with generated MAC also involving these subcompartments, potentially contributing to observed lung injury. Infected mice also had evidence of a systemic increase in complement activity based on C3 and C4 ELISA, APFA, and CH_{50} activity assays, though we found no evidence of substantial complement activation in organs outside the lungs (Figure S9). Overall, these findings suggest that SARS-CoV-2 infection primarily induces a lung-specific complement response.

Whereas our studies, as well as others, demonstrate local production of complement by respiratory epithelial cells,[43,46,52] no *in vivo* model of SARS-CoV-2 has confirmed this finding. Here, we provide evidence that mice infected with SARS2-N501Y$_{MA30}$ have increased transcription of complement-activating genes and decreased expression of complement-regulating genes in the lung. *C3*, *Cfb*, *Cfp*, and *Cfh* are among the most significantly altered, suggesting AP activation in this model of COVID-19 (Figures 2 and 6). Importantly, this AP specific transcriptional data are supported by protein analysis as we observed significant increases in pulmonary FB and Bb increases significantly post-infection (Figure 3B). We also observed increases in transcript abundance for genes associated with the CP. However, a similar pattern of CP upregulation was previously described in COVID-19 patients[66] and might reflect the later time point of 5 dpi for sample collection. This may coincide with the onset of immunocomplex formation and resultant IgM- and IgG-mediated activation of the CP with subsequent C4 cleavage and C3 convertase formation.[37] Thus, CP activation may be a later event rather than the primary driver of complement activation and respiratory disease pathology. Likewise, the increase in serum C4 could reflect its role in the inflammatory response, with liver-derived C4 produced as a non-specific acute phase reactant rather than a specific response to SARS2-N501Y$_{MA30}$ infection. Additionally, we note that while there was no overall significant increase in pulmonary C4, some male mice appeared to have higher C4 levels compared to controls on 2 dpi, and taken with the RNA-seq data, future studies should explore this discrepancy, as identification of the triggering pathway has important mechanistic and therapeutic implications, providing grounds for future research. Importantly, our findings of increased transcription of

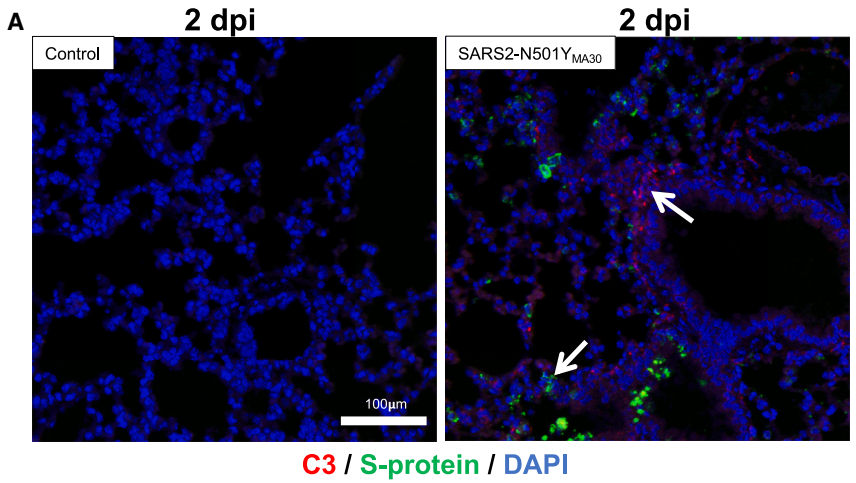

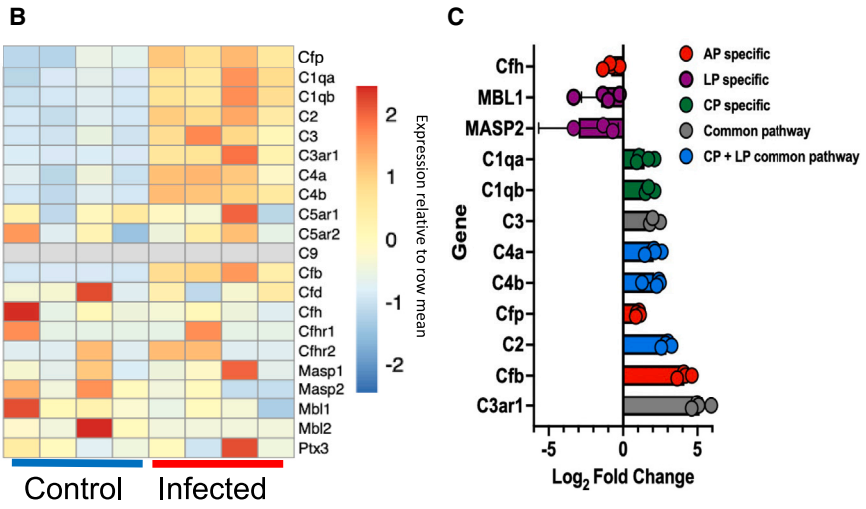

Figure 6. Messenger RNA expression analysis suggests local production of complement proteins in lung tissue following SARS2-N501Y$_{MA30}$ infection

(A) RNAscope for S-protein RNA and C3 RNA in lung tissue sections on 2 dpi following 5,000 PFU of SARS2-N501Y$_{MA30}$. White arrows indicate C3 RNA and SARS2-N501Y$_{MA30}$ S-protein RNA, red = C3, green = S-protein, and blue = DAPI.

(B) Heatmap depicting the results of bulk RNA sequencing for genes associated with complement pathways from lung tissue collected 5 dpi following inoculation with 1,000 PFU SARS2-N501Y$_{MA30}$.

(C) Mean log$_2$ fold change in transcript abundance post-infection. Complement pathway indicated by bar color: red = alternative pathway specific genes, purple = lectin pathway specific genes, green = classical pathway specific genes, gray = common pathway genes, blue = shared classical and lectin pathway genes. *n* = 4. dpi, days post-infection. Error bars represent mean ± SEM.

complement genes within the lungs were not unique to this mouse model of severe COVID-19. We performed analyses of publicly available scRNA-sequencing databases generated from a Syrian hamster model of moderate COVID-19[67] and a database from human COVID-19 patients[68] and found that a similar pattern of increased complement gene transcription in the lungs following SARS-CoV-2 infection was conserved across species and illness severity (Figure S12). Together, these findings support the concept of a locally derived complement response, which may drive lung injury in COVID-19 and warrants future investigation.

Previous studies have suggested SARS-CoV-2 activates complement through direct interaction between viral antigen and complement proteins, or as a cellular response to viral invasion.[42,43] However, our results suggest that complement activation may be induced in a more paracrine or systemic fashion. The significance of this observation is that the complement response is diffuse, involves the entire lung, and induces widespread pulmonary inflammation and cellular injury. Consistent with this pathophysiology, the cytokine profile is one of inflammation that can be driven by the potent anaphylatoxins C3a and C5a binding to their respective receptors as described previously.[69–71] The pattern of gene expression could be consistent with a complement-mediated response via mitochondrial antiviral-signaling protein (MAVS)[65] in which (nuclear factor κB) NF-κB and interferon regulatory factor 3 (IRF3) can be stimulated by C3.[65] A similar cytokine/chemokine pattern can also be associated with C3a and C5a stimulation of direct (C3aR1 and C5aR1) and indirect (potentiation of TLR signal) p38 MAPK inflammatory signaling, inducing NF-κB and activator protein 1 (AP-1) mediated cytokine/chemokine responses.[71] This suggests that following infection with SARS2-N501Y$_{MA30}$, there is complement activation with a subsequent complement-mediated inflammatory response. This inflammation is primarily pulmonary in origin, consistent with our observation that lung tissue had the greatest complement activation following infection. However, these findings are hypothesis generating and further studies are required to understand the links between complement activation and the inflammatory response.

Humans and mice exhibit sex-specific differences in serologic complement responses[72]; whether this baseline difference in AP activity contributes to the more severe disease phenotype in males deserves more investigation. Overall, these findings support the role of locally produced complement driving both lung injury and inflammation in COVID-19.

In summary, our findings provide strong evidence for local, respiratory epithelial cell derived complement activation in a mouse model of COVID-19. This activation occurs primarily via the AP. It is neither dependent on direct interaction with viral antigen,

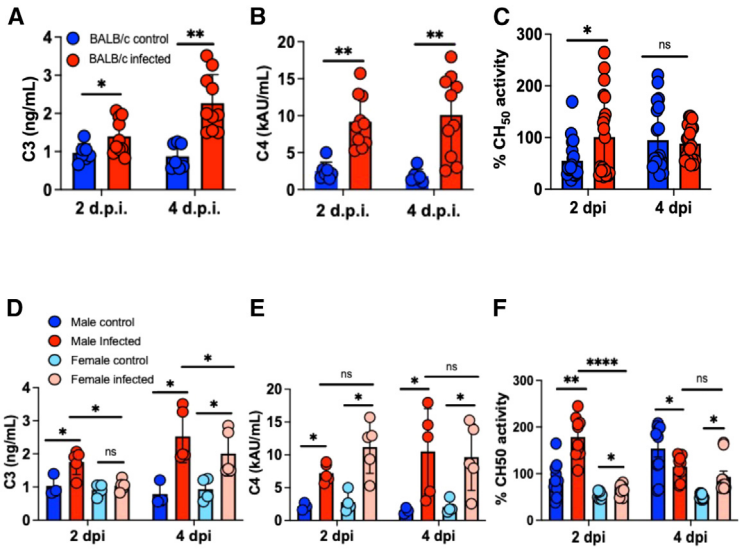

Figure 7. Characterization of systemic complement activity in mice infected with SARS2-N501Y$_{MA30}$

(A and B) Serum C3 and C4 ELISA from control (blue) and infected (red) mice on 2 and 4 dpi.

(C) Serum CH_{50} activity assay from control (blue) and SARS2-N501Y$_{MA30}$ mice (red).

(D–F) Comparison of sex differences by serum ELISA for C3 (D) and C4 (E) on 2 and 4 dpi, with data from sex specific CH_{50} activity assay shown in (F). dpi, days post-infection. Significance determined by one-way ANOVA or unpaired t test, $^{*}p < 0.05$, $^{**}p < 0.01$, $^{****}p < 0.0001$, ns = nonsignificant. C3 and C4 measured from $n = 7$. DMEM and $n = 10$ SARS2-N501Y$_{MA30}$ mice per group. CH_{50} assay from $n = 10$ mice per group, samples run in duplicate. Error bars represent mean ± SEM.

nor is it simply a cellular response to viral invasion. Our observation that C3 activation precedes any cytokine or cellular immune response in the lung supports the concept that both the local and systemic inflammatory responses in COVID-19 are mediated by local complement activation. This work will serve as a foundation for studies addressing the role of complement inhibitors in the treatment of COVID-19. The approach presented here could also be used to explore the role of complement in other forms of infectious and non-infectious acute and chronic lung injury.

Limitations of the study

Our study has limitations. First, while this murine model recapitulates several features of COVID-19, mice are imperfect surrogates for humans and differ significantly in features of pulmonary anatomy, immune system function, and complement activity.[73–75] Second, the data presented come from a single mouse strain, BALB/c. We know that mouse strains respond differently to viral infections, including SARS-CoV-2,[47] and the complement response can have inter-strain variability.[76] Third, our experiments focused on a severe disease phenotype and followed mice over a short period as all infected animals succumbed to infection prior to day 10. Thus, we cannot extrapolate our findings to more mild iterations of disease. Likewise, we are unable to comment on the effect of complement activation in the recovery period or any implications this activation might have on the development and perpetuation of "long-COVID."[77,78] Finally, because our studies focused on describing the mechanism and role of complement activation in a mouse model of COVID-19, we did not explore the impact a deficit of complement, either by pharmaceutical intervention or genetic alteration, has on disease.

RESOURCE AVAILABILITY

Lead contact

Further information and requests for resources and reagents should be directed to and will be fulfilled by the lead contact, Peter J. Szachowicz (peter-szachowicz@uiowa.edu).

Materials availability

All unique/stable reagents generated in this study are available from the lead contact with a completed materials transfer agreement.

Data and code availability

- The supporting data values XLS file includes values for each data point presented in the paper. This manuscript analyzes existing, publicly available data accessible at https://doi.org/10.1038/s41586-021-03569-1 and https://doi.org/10.1038/s41467-021-25030-7 as Gene Expression Omnibus (GEO) as accession numbers GEO: GSE171524 and GEO: GSE162208, respectively. RNA-seq data generated from murine subjects is deposited in the GEO as accession numbers GEO: GSE249304 and RNA-seq data from human airways epithelia culture was deposited at GEO as accession numbers GEO: GSE176121 and GEO: GSE285099.
- The paper does not report original code.
- Any additional information required to reanalyze the data reported in this paper is available from the lead contact upon request.

ACKNOWLEDGMENTS

We would like to thank Paul Morgan, Wioleta Zelek, Ron Taylor, Santiago Rodriguez de Cordoba, and Matthew Pickering for the sharing of reagents, experimental assistance, and helpful discussions that contributed to this manuscript. We would like to thank the Tully family for their support. This work was supported with funding from National Institutes of Health (NIH) (P01 AI-060699), the Center for Gene Therapy of Cystic Fibrosis (P30 DK-54759) (P.B.M.), the University of Iowa Carver College of Medicine COVID-19 Pilot Grant, and the Tully Family Foundation. P.B.M. is supported by the Roy J. Carver Charitable Trust. Carver College of Medicine COVID-19 Grant (P.B.M. and A.P.), and NHLBI 1R01HL163024 (A.P.).

Role of the funding source: The funders of this original research had no role in the study design, writing of the report, interpretation of data, or the decision to submit the paper for publication.

AUTHOR CONTRIBUTIONS

P.J.S., C.W.-L., P.B.M., R.J.H.S., and Y.Z. conceived and designed studies. P.J.S., A.V., C.J.D., S.G., A.A.P., L.M., and C.W.-L. performed experiments. C.J.D. performed ELISA experiments. S.G., A.T., B.X., P.J.S., and A.A.P. performed RNA-seq and data analysis. A.T. assisted with secondary analysis of published scRNA-seq data. J.R.B., T.J.B., and P.J.S. contributed to cytokine

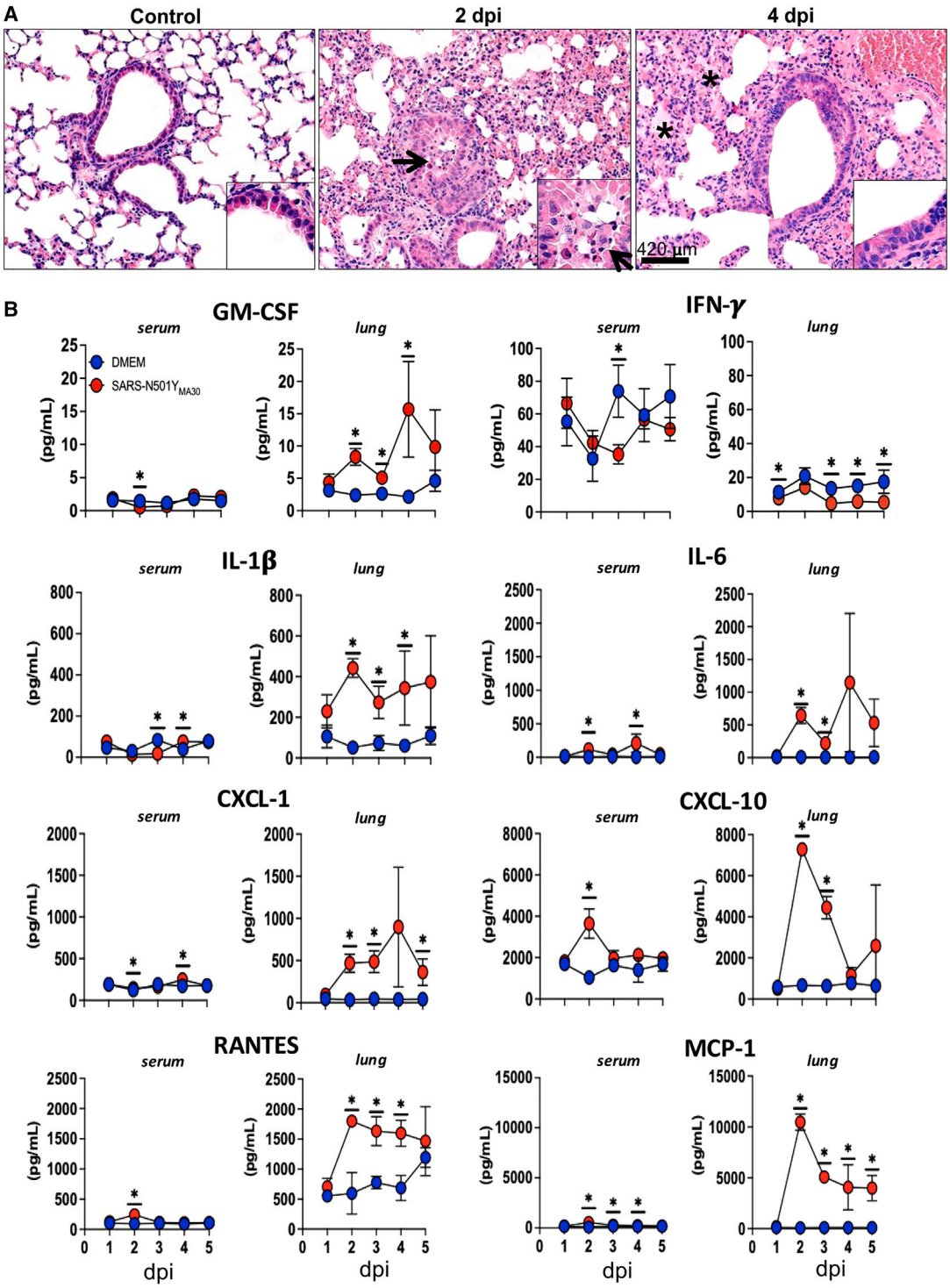

Figure 8. Lung histopathology and inflammatory response is consistent with complement mediated disease

(A) Representative images of H&E staining of lung tissue from histopathologic exam. Samples from control and infected mice on 2 and 4 dpi demonstrate cellular infiltrates (2 dpi) (black arrows) and edema (4 dpi) (black asterisks). Insets show airways with intralumenal cellular debris and surrounding lymphocytic and myeloid cell types noted on 4 dpi, $n = 3$ mice per time point.

(B) Serum and lung cytokine profiling for 1–5 dpi, title above graph in each column indicates whether sample is from serum or lung homogenate. $n = 3$ mice per group at each time point. DMEM, Dulbecco's modified Eagle's medium; dpi, days post-infection. Significance determined by unpaired t test,*$p < 0.05$. Error bars represent mean ± SEM.

assay. D.K.M. performed histopathology and viral IHC. A.V. performed RNAscope. S.P. provided valuable insights in discussions and helped design experiments. P.J.S., P.B.M., Y.Z., and R.J.H.S. analyzed data. P.J.S. wrote the manuscript with editorial support from P.B.M. and R.J.H.S. All authors approved of the manuscript.

DECLARATION OF INTERESTS

The authors declare no competing interests.

STAR★METHODS

Detailed methods are provided in the online version of this paper and include the following:

- KEY RESOURCES TABLE
- EXPERIMENTAL MODEL AND SUBJECT DETAILS
  - Mice, human tissue, cells, and virus
  - Sample-size estimation
  - Sex as a biological variable
  - Ethics statement
  - Animal studies
  - Human airway epithelial cells and cell line cultures
  - SARS2-N501Y$_{MA30}$ virus
- METHOD DETAILS
  - SARS-CoV-2 infection
  - Quantitative histopathology and immunohistochemistry
  - Antibodies and immunolocalization
  - Bioplex cytokine profiling
  - Virus titers
  - Western blot analysis
  - ELISA
  - Cytokine stimulation of human airway epithelial cells
  - Mouse lung bulk RNA sequencing
  - Human airway epithelial cell RNA sequencing
  - RNAscope
- QUANTIFICATION AND STATISTICAL ANALYSIS

SUPPLEMENTAL INFORMATION

Supplemental information can be found online at https://doi.org/10.1016/j.isci.2025.111930.

Received: July 15, 2024
Revised: October 21, 2024
Accepted: January 27, 2025
Published: February 1, 2025

REFERENCES

1. Yuki, K., Fujiogi, M., and Koutsogiannaki, S. (2020). COVID-19 pathophysiology: A review. Clin. Immunol. *215*, 108427. https://doi.org/10.1016/j.clim.2020.108427.
2. Baden, L.R., El Sahly, H.M., Essink, B., Kotloff, K., Frey, S., Novak, R., Diemert, D., Spector, S.A., Rouphael, N., Creech, C.B., et al. (2021). Efficacy and Safety of the mRNA-1273 SARS-CoV-2 Vaccine. N Engl J Med *384*, 403–416. https://doi.org/10.1056/NEJMoa2035389.
3. Thomas, S.J., Moreira, E.D., Jr., Kitchin, N., Absalon, J., Gurtman, A., Lockhart, S., Perez, J.L., Pérez Marc, G., Polack, F.P., Zerbini, C., et al. (2021). Safety and Efficacy of the BNT162b2 mRNA Covid-19 Vaccine through 6 Months. N. Engl. J. Med. *385*, 1761–1773. https://doi.org/10.1056/NEJMoa2110345.
4. Hammond, J., Leister-Tebbe, H., Gardner, A., Abreu, P., Bao, W., Wisemandle, W., Baniecki, M., Hendrick, V.M., Damle, B., Simón-Campos, A., et al. (2022). Oral Nirmatrelvir for High-Risk, Nonhospitalized Adults with Covid-19. N. Engl. J. Med. *386*, 1397–1408. https://doi.org/10.1056/NEJMoa2118542.
5. The RECOVERY Collaborative Group (2021). Dexamethasone in Hospitalized Patients with Covid-19. N Engl J Med *384*, 693–704. https://doi.org/10.1056/NEJMoa2021436.
6. Rosas, I.O., Bräu, N., Waters, M., Go, R.C., Hunter, B.D., Bhagani, S., Skiest, D., Aziz, M.S., Cooper, N., Douglas, I.S., et al. (2021). Tocilizumab in Hospitalized Patients with Severe Covid-19 Pneumonia. N. Engl. J. Med. *384*, 1503–1516. https://doi.org/10.1056/NEJMoa2028700.
7. Marconi, V.C., Ramanan, A.V., de Bono, S., Kartman, C.E., Krishnan, V., Liao, R., Piruzeli, M.L.B., Goldman, J.D., Alatorre-Alexander, J., de Cassia Pellegrini, R., et al. (2021). Efficacy and safety of baricitinib for the treatment of hospitalised adults with COVID-19 (COV-BARRIER): a randomised, double-blind, parallel-group, placebo-controlled phase 3 trial. Lancet. Respir. Med. *9*, 1407–1418. https://doi.org/10.1016/S2213-2600(21)00331-3.
8. Carabelli, A.M., Peacock, T.P., Thorne, L.G., Harvey, W.T., Hughes, J., COVID-19 Genomics UK Consortium; Peacock, S.J., Barclay, W.S., de Silva, T.I., Towers, G.J., and Robertson, D.L. (2023). SARS-CoV-2 variant biology: immune escape, transmission and fitness. Nat. Rev. Microbiol. *21*, 162–177. https://doi.org/10.1038/s41579-022-00841-7.
9. Pagani, I., Ghezzi, S., Alberti, S., Poli, G., and Vicenzi, E. (2023). Origin and evolution of SARS-CoV-2. Eur. Phys. J. Plus *138*, 157. https://doi.org/10.1140/epjp/s13360-023-03719-6.
10. Magro, C., Mulvey, J.J., Berlin, D., Nuovo, G., Salvatore, S., Harp, J., Baxter-Stoltzfus, A., and Laurence, J. (2020). Complement associated microvascular injury and thrombosis in the pathogenesis of severe COVID-19 infection: A report of five cases. Transl. Res. *220*, 1–13. https://doi.org/10.1016/j.trsl.2020.04.007.
11. Perico, L., Benigni, A., Casiraghi, F., Ng, L.F.P., Renia, L., and Remuzzi, G. (2021). Immunity, endothelial injury and complement-induced coagulopathy in COVID-19. Nat. Rev. Nephrol. *17*, 46–64. https://doi.org/10.1038/s41581-020-00357-4.
12. Cugno, M., Meroni, P.L., Gualtierotti, R., Griffini, S., Grovetti, E., Torri, A., Lonati, P., Grossi, C., Borghi, M.O., Novembrino, C., et al. (2021). Complement activation and endothelial perturbation parallel COVID-19 severity and activity. J. Autoimmun. *116*, 102560. https://doi.org/10.1016/j.jaut.2020.102560.
13. Fujimura, Y., and Holland, L.Z. (2022). COVID-19 microthrombosis: unusually large VWF multimers are a platform for activation of the alternative complement pathway under cytokine storm. Int. J. Hematol. *115*, 457–469. https://doi.org/10.1007/s12185-022-03324-w.
14. Kim, J.S., Lee, J.Y., Yang, J.W., Lee, K.H., Effenberger, M., Szpirt, W., Kronbichler, A., and Shin, J.I. (2021). Immunopathogenesis and treatment of cytokine storm in COVID-19. Theranostics *11*, 316–329. https://doi.org/10.7150/thno.49713.
15. Mahmudpour, M., Roozbeh, J., Keshavarz, M., Farrokhi, S., and Nabipour, I. (2020). COVID-19 cytokine storm: The anger of inflammation. Cytokine *133*, 155151. https://doi.org/10.1016/j.cyto.2020.155151.
16. Skendros, P., Mitsios, A., Chrysanthopoulou, A., Mastellos, D.C., Metallidis, S., Rafailidis, P., Ntinopoulou, M., Sertaridou, E., Tsironidou, V., Tsigalou, C., et al. (2020). Complement and tissue factor-enriched neutrophil extracellular traps are key drivers in COVID-19 immunothrombosis. J. Clin. Invest. *130*, 6151–6157. https://doi.org/10.1172/JCI141374.
17. Georg, P., Astaburuaga-García, R., Bonaguro, L., Brumhard, S., Michalick, L., Lippert, L.J., Kostevc, T., Gäbel, C., Schneider, M., Streitz, M., et al. (2022). Complement activation induces excessive T cell cytotoxicity in severe COVID-19. Cell *185*, 493–512.e25. https://doi.org/10.1016/j.cell.2021.12.040.
18. Zelek, W.M., and Harrison, R.A. (2023). Complement and COVID-19: Three years on, what we know, what we don't know, and what we ought to know. Immunobiology *228*, 152393. https://doi.org/10.1016/j.imbio.2023.152393.

19. Nesargikar, P.N., Spiller, B., and Chavez, R. (2012). The complement system: history, pathways, cascade and inhibitors. Eur. J. Microbiol. Immunol. *2*, 103–111. https://doi.org/10.1556/EuJMI.2.2012.2.2.

20. Mastellos, D.C., Hajishengallis, G., and Lambris, J.D. (2024). A guide to complement biology, pathology and therapeutic opportunity. Nat. Rev. Immunol. *24*, 118–141. https://doi.org/10.1038/s41577-023-00926-1.

21. Carroll, M.C. (2008). Complement and humoral immunity. Vaccine *26*, I28–I33. https://doi.org/10.1016/j.vaccine.2008.11.022.

22. Dunkelberger, J.R., and Song, W.C. (2010). Complement and its role in innate and adaptive immune responses. Cell Res. *20*, 34–50. https://doi.org/10.1038/cr.2009.139.

23. Killick, J., Morisse, G., Sieger, D., and Astier, A.L. (2018). Complement as a regulator of adaptive immunity. Semin. Immunopathol. *40*, 37–48. https://doi.org/10.1007/s00281-017-0644-y.

24. Zheng, R., Zhang, Y., Zhang, K., Yuan, Y., Jia, S., and Liu, J. (2022). The Complement System, Aging, and Aging-Related Diseases. Int. J. Mol. Sci. *23*, 8689. https://doi.org/10.3390/ijms23158689.

25. Hess, C., and Kemper, C. (2016). Complement-Mediated Regulation of Metabolism and Basic Cellular Processes. Immunity *45*, 240–254. https://doi.org/10.1016/j.immuni.2016.08.003.

26. Fishelson, Z., Attali, G., and Mevorach, D. (2001). Complement and apoptosis. Mol. Immunol. *38*, 207–219. https://doi.org/10.1016/s0161-5890(01)00055-4.

27. Liszewski, M.K., Kolev, M., Le Friec, G., Leung, M., Bertram, P.G., Fara, A.F., Subias, M., Pickering, M.C., Drouet, C., Meri, S., et al. (2013). Intracellular complement activation sustains T cell homeostasis and mediates effector differentiation. Immunity *39*, 1143–1157. https://doi.org/10.1016/j.immuni.2013.10.018.

28. King, B.C., Kulak, K., Krus, U., Rosberg, R., Golec, E., Wozniak, K., Gomez, M.F., Zhang, E., O'Connell, D.J., Renström, E., and Blom, A.M. (2019). Complement Component C3 Is Highly Expressed in Human Pancreatic Islets and Prevents beta Cell Death via ATG16L1 Interaction and Autophagy Regulation. Cell Metab. *29*, 202–210.e6. https://doi.org/10.1016/j.cmet.2018.09.009.

29. Chaudhary, N., Jayaraman, A., Reinhardt, C., Campbell, J.D., and Bosmann, M. (2022). A single-cell lung atlas of complement genes identifies the mesothelium and epithelium as prominent sources of extrahepatic complement proteins. Mucosal Immunol. *15*, 927–939. https://doi.org/10.1038/s41385-022-00534-7.

30. Kopf, M., Abel, B., Gallimore, A., Carroll, M., and Bachmann, M.F. (2002). Complement component C3 promotes T-cell priming and lung migration to control acute influenza virus infection. Nat. Med. *8*, 373–378. https://doi.org/10.1038/nm0402-373.

31. Jiang, Y., Li, J., Teng, Y., Sun, H., Tian, G., He, L., Li, P., Chen, Y., Guo, Y., Li, J., et al. (2019). Complement Receptor C5aR1 Inhibition Reduces Pyroptosis in hDPP4-Transgenic Mice Infected with MERS-CoV. Viruses *11*, 39. https://doi.org/10.3390/v11010039.

32. Gralinski, L.E., Sheahan, T.P., Morrison, T.E., Menachery, V.D., Jensen, K., Leist, S.R., Whitmore, A., Heise, M.T., and Baric, R.S. (2018). Complement Activation Contributes to Severe Acute Respiratory Syndrome Coronavirus Pathogenesis. mBio *9*, e01753-18. https://doi.org/10.1128/mBio.01753-18.

33. Ramlall, V., Thangaraj, P.M., Meydan, C., Foox, J., Butler, D., Kim, J., May, B., De Freitas, J.K., Glicksberg, B.S., Mason, C.E., et al. (2020). Immune complement and coagulation dysfunction in adverse outcomes of SARS-CoV-2 infection. Nat. Med. *26*, 1609–1615. https://doi.org/10.1038/s41591-020-1021-2.

34. Ma, L., Sahu, S.K., Cano, M., Kuppuswamy, V., Bajwa, J., McPhatter, J., Pine, A., Meizlish, M.L., Goshua, G., Chang, C.H., et al. (2021). Increased complement activation is a distinctive feature of severe SARS-CoV-2 infection. Sci. Immunol. *6*, eabh2259. https://doi.org/10.1126/sciimmunol.abh2259.

35. Messner, C.B., Demichev, V., Wendisch, D., Michalick, L., White, M., Freiwald, A., Textoris-Taube, K., Vernardis, S.I., Egger, A.S., Kreidl, M., et al. (2020). Ultra-High-Throughput Clinical Proteomics Reveals Classifiers of COVID-19 Infection. Cell Syst. *11*, 11–24.e4. https://doi.org/10.1016/j.cels.2020.05.012.

36. Gisby, J.S., Buang, N.B., Papadaki, A., Clarke, C.L., Malik, T.H., Medjeral-Thomas, N., Pinheiro, D., Mortimer, P.M., Lewis, S., Sandhu, E., et al. (2022). Multi-omics identify falling LRRC15 as a COVID-19 severity marker and persistent pro-thrombotic signals in convalescence. Nat. Commun. *13*, 7775. https://doi.org/10.1038/s41467-022-35454-4.

37. Siggins, M.K., Davies, K., Fellows, R., Thwaites, R.S., Baillie, J.K., Semple, M.G., Openshaw, P.J.M., Zelek, W.M., Harris, C.L., and Morgan, B.P.; ISARIC4C Investigators (2023). Alternative pathway dysregulation in tissues drives sustained complement activation and predicts outcome across the disease course in COVID-19. Immunology *168*, 473–492. https://doi.org/10.1111/imm.13585.

38. Holter, J.C., Pischke, S.E., de Boer, E., Lind, A., Jenum, S., Holten, A.R., Tonby, K., Barratt-Due, A., Sokolova, M., Schjalm, C., et al. (2020). Systemic complement activation is associated with respiratory failure in COVID-19 hospitalized patients. Proc. Natl. Acad. Sci. USA *117*, 25018–25025. https://doi.org/10.1073/pnas.2010540117.

39. Defendi, F., Leroy, C., Epaulard, O., Clavarino, G., Vilotitch, A., Le Marechal, M., Jacob, M.C., Raskovalova, T., Pernollet, M., Le Gouellec, A., et al. (2021). Complement Alternative and Mannose-Binding Lectin Pathway Activation Is Associated With COVID-19 Mortality. Front. Immunol. *12*, 742446. https://doi.org/10.3389/fimmu.2021.742446.

40. Ali, Y.M., Ferrari, M., Lynch, N.J., Yaseen, S., Dudler, T., Gragerov, S., Demopulos, G., Heeney, J.L., and Schwaeble, W.J. (2021). Lectin Pathway Mediates Complement Activation by SARS-CoV-2 Proteins. Front. Immunol. *12*, 714511. https://doi.org/10.3389/fimmu.2021.714511.

41. Savitt, A.G., Manimala, S., White, T., Fandaros, M., Yin, W., Duan, H., Xu, X., Geisbrecht, B.V., Rubenstein, D.A., Kaplan, A.P., et al. (2021). SARS-CoV-2 Exacerbates COVID-19 Pathology Through Activation of the Complement and Kinin Systems. Front. Immunol. *12*, 767347. https://doi.org/10.3389/fimmu.2021.767347.

42. Yu, J., Yuan, X., Chen, H., Chaturvedi, S., Braunstein, E.M., and Brodsky, R.A. (2020). Direct activation of the alternative complement pathway by SARS-CoV-2 spike proteins is blocked by factor D inhibition. Blood *136*, 2080–2089. https://doi.org/10.1182/blood.2020008248.

43. Yan, B., Freiwald, T., Chauss, D., Wang, L., West, E., Mirabelli, C., Zhang, C.J., Nichols, E.M., Malik, N., Gregory, R., et al. (2021). SARS-CoV-2 drives JAK1/2-dependent local complement hyperactivation. Sci. Immunol. *6*, eabg0833. https://doi.org/10.1126/sciimmunol.abg0833.

44. Stravalaci, M., Pagani, I., Paraboschi, E.M., Pedotti, M., Doni, A., Scavello, F., Mapelli, S.N., Sironi, M., Perucchini, C., Varani, L., et al. (2022). Recognition and inhibition of SARS-CoV-2 by humoral innate immunity pattern recognition molecules. Nat. Immunol. *23*, 275–286. https://doi.org/10.1038/s41590-021-01114-w.

45. Kulkarni, H.S., Liszewski, M.K., Brody, S.L., and Atkinson, J.P. (2018). The complement system in the airway epithelium: An overlooked host defense mechanism and therapeutic target? J. Allergy Clin. Immunol. *141*, 1582–1586.e1. https://doi.org/10.1016/j.jaci.2017.11.046.

46. Bartlett, J.A., Albertolle, M.E., Wohlford-Lenane, C., Pezzulo, A.A., Zabner, J., Niles, R.K., Fisher, S.J., McCray, P.B., Jr., and Williams, K.E. (2013). Protein composition of bronchoalveolar lavage fluid and airway surface liquid from newborn pigs. Am. J. Physiol. Lung Cell. Mol. Physiol. *305*, L256–L266. https://doi.org/10.1152/ajplung.00056.2013.

47. Wong, L.Y.R., Zheng, J., Wilhelmsen, K., Li, K., Ortiz, M.E., Schnicker, N.J., Thurman, A., Pezzulo, A.A., Szachowicz, P.J., Li, P., et al. (2022). Eicosanoid signalling blockade protects middle-aged mice from severe COVID-19. Nature *605*, 146–151. https://doi.org/10.1038/s41586-022-04630-3.

48. Jiang, R.D., Liu, M.Q., Chen, Y., Shan, C., Zhou, Y.W., Shen, X.R., Li, Q., Zhang, L., Zhu, Y., Si, H.R., et al. (2020). Pathogenesis of SARS-CoV-2 in

Transgenic Mice Expressing Human Angiotensin-Converting Enzyme 2. Cell *182*, 50–58.e8. https://doi.org/10.1016/j.cell.2020.05.027.

49. Niederreiter, J., Eck, C., Ries, T., Hartmann, A., Märkl, B., Büttner-Herold, M., Amann, K., and Daniel, C. (2022). Complement Activation via the Lectin and Alternative Pathway in Patients With Severe COVID-19. Front. Immunol. *13*, 835156. https://doi.org/10.3389/fimmu.2022.835156.

50. Cho, J.L., Villacreses, R., Nagpal, P., Guo, J., Pezzulo, A.A., Thurman, A.L., Hamzeh, N.Y., Blount, R.J., Fortis, S., Hoffman, E.A., et al. (2022). Quantitative Chest CT Assessment of Small Airways Disease in Post-Acute SARS-CoV-2 Infection. Radiology *304*, 185–192. https://doi.org/10.1148/radiol.212170.

51. Borczuk, A.C., Salvatore, S.P., Seshan, S.V., Patel, S.S., Bussel, J.B., Mostyka, M., Elsoukkary, S., He, B., Del Vecchio, C., Fortarezza, F., et al. (2020). COVID-19 pulmonary pathology: a multi-institutional autopsy cohort from Italy and New York City. Mod. Pathol. *33*, 2156–2168. https://doi.org/10.1038/s41379-020-00661-1.

52. Sahu, S.K., Ozantürk, A.N., Kulkarni, D.H., Ma, L., Barve, R.A., Dannull, L., Lu, A., Starick, M., McPhatter, J., Garnica, L., et al. (2023). Lung epithelial cell-derived C3 protects against pneumonia-induced lung injury. Sci. Immunol. *8*, eabp9547. https://doi.org/10.1126/sciimmunol.abp9547.

53. Mukherjee, S., Lindell, D.M., Berlin, A.A., Morris, S.B., Shanley, T.P., Hershenson, M.B., and Lukacs, N.W. (2011). IL-17-induced pulmonary pathogenesis during respiratory viral infection and exacerbation of allergic disease. Am. J. Pathol. *179*, 248–258. https://doi.org/10.1016/j.ajpath.2011.03.003.

54. Message, S.D., and Johnston, S.L. (2004). Host defense function of the airway epithelium in health and disease: clinical background. J. Leukoc. Biol. *75*, 5–17. https://doi.org/10.1189/jlb.0703315.

55. See, H., and Wark, P. (2008). Innate immune response to viral infection of the lungs. Paediatr. Respir. Rev. *9*, 243–250. https://doi.org/10.1016/j.prrv.2008.04.001.

56. Tang, Y., Liu, J., Zhang, D., Xu, Z., Ji, J., and Wen, C. (2020). Cytokine Storm in COVID-19: The Current Evidence and Treatment Strategies. Front. Immunol. *11*, 1708. https://doi.org/10.3389/fimmu.2020.01708.

57. Mortaz, E., Tabarsi, P., Jamaati, H., Dalil Roofchayee, N., Dezfuli, N.K., Hashemian, S.M., Moniri, A., Marjani, M., Malekmohammad, M., Mansouri, D., et al. (2021). Increased Serum Levels of Soluble TNF-alpha Receptor Is Associated With ICU Mortality in COVID-19 Patients. Front. Immunol. *12*, 592727. https://doi.org/10.3389/fimmu.2021.592727.

58. Katz, Y., Revel, M., and Strunk, R.C. (1989). Interleukin 6 stimulates synthesis of complement proteins factor B and C3 in human skin fibroblasts. Eur. J. Immunol. *19*, 983–988. https://doi.org/10.1002/eji.1830190605.

59. Moon, M.R., Parikh, A.A., Pritts, T.A., Kane, C., Fischer, J.E., Salzman, A.L., and Hasselgren, P.O. (2000). Interleukin-1beta induces complement component C3 and IL-6 production at the basolateral and apical membranes in a human intestinal epithelial cell line. Shock *13*, 374–378. https://doi.org/10.1097/00024382-200005000-00005.

60. Paschou, S.A., Psaltopoulou, T., Halvatsiotis, P., Raptis, A., Vlachopoulos, C.V., and Dimopoulos, M.A. (2022). Gender differences in COVID-19. Maturitas *161*, 72–73. https://doi.org/10.1016/j.maturitas.2022.03.004.

61. Hu, B., Huang, S., and Yin, L. (2021). The cytokine storm and COVID-19. J. Med. Virol. *93*, 250–256. https://doi.org/10.1002/jmv.26232.

62. Corcoran, J.A., and Napier, B.A. (2022). C3aR plays both sides in regulating resistance to bacterial infections. PLoS Pathog. *18*, e1010657. https://doi.org/10.1371/journal.ppat.1010657.

63. Jacob, A., Hack, B., Bai, T., Brorson, J.R., Quigg, R.J., and Alexander, J.J. (2010). Inhibition of C5a receptor alleviates experimental CNS lupus. J. Neuroimmunol. *221*, 46–52. https://doi.org/10.1016/j.jneuroim.2010.02.011.

64. Wang, R., Xiao, H., Guo, R., Li, Y., and Shen, B. (2015). The role of C5a in acute lung injury induced by highly pathogenic viral infections. Emerg. Microbes Infect. *4*, e28. https://doi.org/10.1038/emi.2015.28.

65. Tam, J.C.H., Bidgood, S.R., McEwan, W.A., and James, L.C. (2014). Intracellular sensing of complement C3 activates cell autonomous immunity. Science *345*, 1256070. https://doi.org/10.1126/science.1256070.

66. Satyam, A., Tsokos, M.G., Brook, O.R., Hecht, J.L., Moulton, V.R., and Tsokos, G.C. (2021). Activation of classical and alternative complement pathways in the pathogenesis of lung injury in COVID-19. Clin. Immunol. *226*, 108716. https://doi.org/10.1016/j.clim.2021.108716.

67. Nouailles, G., Wyler, E., Pennitz, P., Postmus, D., Vladimirova, D., Kazmierski, J., Pott, F., Dietert, K., Muelleder, M., Farztdinov, V., et al. (2021). Temporal omics analysis in Syrian hamsters unravel cellular effector responses to moderate COVID-19. Nat. Commun. *12*, 4869. https://doi.org/10.1038/s41467-021-25030-7.

68. Melms, J.C., Biermann, J., Huang, H., Wang, Y., Nair, A., Tagore, S., Katsyv, I., Rendeiro, A.F., Amin, A.D., Schapiro, D., et al. (2021). A molecular single-cell lung atlas of lethal COVID-19. Nature *595*, 114–119. https://doi.org/10.1038/s41586-021-03569-1.

69. Gao, S., Cui, Z., and Zhao, M.H. (2020). The Complement C3a and C3a Receptor Pathway in Kidney Diseases. Front. Immunol. *11*, 1875. https://doi.org/10.3389/fimmu.2020.01875.

70. Posch, W., Vosper, J., Noureen, A., Zaderer, V., Witting, C., Bertacchi, G., Gstir, R., Filipek, P.A., Bonn, G.K., Huber, L.A., et al. (2021). C5aR inhibition of nonimmune cells suppresses inflammation and maintains epithelial integrity in SARS-CoV-2-infected primary human airway epithelia. J. Allergy Clin. Immunol. *147*, 2083–2097.e6. https://doi.org/10.1016/j.jaci.2021.03.038.

71. Reis, E.S., Mastellos, D.C., Hajishengallis, G., and Lambris, J.D. (2019). New insights into the immune functions of complement. Nat. Rev. Immunol. *19*, 503–516. https://doi.org/10.1038/s41577-019-0168-x.

72. Gaya da Costa, M., Poppelaars, F., van Kooten, C., Mollnes, T.E., Tedesco, F., Würzner, R., Trouw, L.A., Truedsson, L., Daha, M.R., Roos, A., and Seelen, M.A. (2018). Age and Sex-Associated Changes of Complement Activity and Complement Levels in a Healthy Caucasian Population. Front. Immunol. *9*, 2664. https://doi.org/10.3389/fimmu.2018.02664.

73. Basil, M.C., and Morrisey, E.E. (2020). Lung regeneration: a tale of mice and men. Semin. Cell Dev. Biol. *100*, 88–100. https://doi.org/10.1016/j.semcdb.2019.11.006.

74. Mestas, J., and Hughes, C.C.W. (2004). Of mice and not men: differences between mouse and human immunology. J. Immunol. *172*, 2731–2738. https://doi.org/10.4049/jimmunol.172.5.2731.

75. Ueda, Y., Gullipalli, D., and Song, W.C. (2016). Modeling complement-driven diseases in transgenic mice: Values and limitations. Immunobiology *221*, 1080–1090. https://doi.org/10.1016/j.imbio.2016.06.007.

76. Ong, G.L., and Mattes, M.J. (1989). Mouse strains with typical mammalian levels of complement activity. J. Immunol. Methods *125*, 147–158. https://doi.org/10.1016/0022-1759(89)90088-4.

77. Cervia-Hasler, C., Brüningk, S.C., Hoch, T., Fan, B., Muzio, G., Thompson, R.C., Ceglarek, L., Meledin, R., Westermann, P., Emmenegger, M., et al. (2024). Persistent complement dysregulation with signs of thromboinflammation in active Long Covid. Science *383*, eadg7942. https://doi.org/10.1126/science.adg7942.

78. Aschman, T., Wyler, E., Baum, O., Hentschel, A., Rust, R., Legler, F., Preusse, C., Meyer-Arndt, L., Büttnerova, I., Förster, A., et al. (2023). Post-COVID exercise intolerance is associated with capillary alterations and immune dysregulations in skeletal muscles. Acta Neuropathol. Commun. *11*, 193. https://doi.org/10.1186/s40478-023-01662-2.

79. Karp, P.H., Moninger, T.O., Weber, S.P., Nesselhauf, T.S., Launspach, J.L., Zabner, J., and Welsh, M.J. (2002). An in vitro model of differentiated human airway epithelia. Methods for establishing primary cultures. Methods Mol. Biol. *188*, 115–137. https://doi.org/10.1385/1-59259-185-X.

80. Meyerholz, D.K., and Beck, A.P. (2018). Principles and approaches for reproducible scoring of tissue stains in research. Lab. Invest. *98*, 844–855. https://doi.org/10.1038/s41374-018-0057-0.

81. Ortiz, M.E., Thurman, A., Pezzulo, A.A., Leidinger, M.R., Klesney-Tait, J.A., Karp, P.H., Tan, P., Wohlford-Lenane, C., McCray, P.B., Jr., and Meyerholz, D.K. (2020). Heterogeneous expression of the SARS-Coronavirus-2 receptor ACE2 in the human respiratory tract. EBioMedicine *60*, 102976. https://doi.org/10.1016/j.ebiom.2020.102976.

82. Meyerholz, D.K., Lambertz, A.M., and McCray, P.B., Jr. (2016). Dipeptidyl Peptidase 4 Distribution in the Human Respiratory Tract: Implications for the Middle East Respiratory Syndrome. Am. J. Pathol. *186*, 78–86. https://doi.org/10.1016/j.ajpath.2015.09.014.

83. Gilley, A., Boly, T.J., Paden, A., and Bermick, J. (2024). Neonatal immune cells have heightened responses following in-utero exposure to chorioamnionitis or COVID-19. Pediatr. Res. *95*, 1483–1492. https://doi.org/10.1038/s41390-023-02888-5.

84. Bray, N.L., Pimentel, H., Melsted, P., and Pachter, L. (2016). Near-optimal probabilistic RNA-seq quantification. Nat. Biotechnol. *34*, 525–527. https://doi.org/10.1038/nbt.3519.

85. Soneson, C., Love, M.I., and Robinson, M.D. (2015). Differential analyses for RNA-seq: transcript-level estimates improve gene-level inferences. F1000Res. *4*, 1521. https://doi.org/10.12688/f1000research.7563.2.

86. Ge, S.X., Son, E.W., and Yao, R. (2018). iDEP: an integrated web application for differential expression and pathway analysis of RNA-Seq data. BMC Bioinformatics *19*, 534. https://doi.org/10.1186/s12859-018-2486-6.

STAR★METHODS

KEY RESOURCES TABLE

REAGENT or RESOURCE	SOURCE	IDENTIFIER
Antibodies		
SARS-CoV-2 (2019-nCoV) Nucleocapsid	Sino Biological	#40588-T62; RRID:AB_3064900
Anti-mouse C3	MP Biomedicals	#55463; RRID: AB_3675783
Anti-mouse C9	Hycult	#HM1134-20UG; RRID: AB_3675784
Anti-mouse alpha-tubulin	Cell signaling	#5335S; RRID: AB_3675785
Anti-HopE-1	Santa Cruz	#sc-398703; RRID: AB_2687966
Anti-mouse vWF	Millipore	#AB7356; RRID: AB_92216
Anti-human FB	Quidel	#A311; RRID: AB_452512
Anti-mouse C4	Abcam	#ab11863; RRID: AB_2290611
SARS-CoV-2 Nucleocapsid	Sino Biological	#40143-T62; RRID: AB_2892769
Anti-vinculin	Invitrogen	#700062; RRID: AB_2532280
Alexa Fluor 546 Phalloidin	Invitrogen	#A22283; RRID: AB_3675787
Donkey anti-mouse goat Alexa Fluor 488	Invitrogen	#A11055; RRID: AB_3675790
Goat anti-mouse Alexa Fluor 546	Invitrogen	#A11003; RRID: AB_3675791
Donkey anti-rabbit Alexa Fluor 564	Invitrogen	#A10040; RRID: AB_2534016
Bacterial and virus strains		
SARS2-N501Y_{MA30}	University of Iowa	N/A
SARS-CoV-2 (strain2019 n-CoV/USA_WA1/2020)	CDC/BEI Resources	#NR52281
Biological samples		
Human airway epithelia	University of Iowa Tissue and Cell Culture Core	N/A
Chemicals, peptides, and recombinant proteins		
C3	Complement Technology	#A113
Factor B	Complement Technology	#A135
Factor Bb	Complement Technology	#A155
Critical commercial assays		
Bioplex Express Kit - mouse	Biorad	M60009RDPD
RNeasy plus mini-kit	Qiagen	#74134
mRNA sample preparation kit	Illumina	#RS-122-2101
RNAscope Target Retrieval	ACD	#322000
Mouse C3 ELISA	Aviva System Biology	Version 4.0 Lot #KF0338
Mouse C4 ELISA	Hycult	HK217
Mouse APFA	Hycult	HIT422
Mouse CH_{50}	Hycult	HIT420
Deposited data		
Mouse lung RNA-seq	University of Iowa	GSE249304
Human airway epithelia RNA-seq	University of Iowa	GSE176121 and GSE285099
Analyzed public data		
Syrian hamster lung RNA-seq	Columbia University	GEO: GSE171524
Experimental models: Cell lines		
Vero E6	ATCC	#CRL-1586, RRID:CVC_0574
Experimental models: Organisms/strains		
Mouse: BALB/c	Charles River	BALB/cAnNCrl

(*Continued on next page*)

Continued

REAGENT or RESOURCE	SOURCE	IDENTIFIER
Software and algorithms		
GraphPad Prism	GraphPad	v10
ImageJ	FIJI	v2.3.0/1.53q
BioRender	BioRender.com	N/A
Kallisto	https://github.com/pachterlab/kallisto	v0.50.0
tximport	Bioconductor	v1.10.1
R	The R Project	v3.5.1
DESeq2	Bioconductor	v1.30.1
iDEP	South Dakota State University	v0.92
Ggplot2	Tidyverse	v3.3.3
pheatmap	The R Project	v1.0.12

EXPERIMENTAL MODEL AND SUBJECT DETAILS

Mice, human tissue, cells, and virus

Replicates

All mouse and human cell culture experiments were replicated at least one time unless otherwise indicated. All reported results are substantiated by repetition with sample sizes large enough to differentiate between independent biological data points and technical replicates.

Sample-size estimation

Based on pilot data, we predicted 100% mortality in BALB/c mice exposed to SARS2-N501Y$_{MA30}$ when compared to controls. Thus, we calculate that a sample size of 10 mice per group (5 males and 5 females) would be needed for a power of 80%. In our experience, this number is sufficient to determine whether a significant difference exists between groups, and we planned to repeat experiments with larger sample sizes if statistical analysis of our results suggested the experiment was under-powered.

Sex as a biological variable

This study examined male and female mice, and sex-dimorphic effects are reported. Our study examined cell cultures taken from male and female donors, and similar findings are reported for both sexes.

Ethics statement

Primary airway epithelia from human donors were isolated from discarded tissue, autopsy, or surgical specimens. Cells were provided by The University of Iowa *In Vitro* Models and Cell Culture Core Repository. Information that could be used to identify a subject was not provided. All studies involving human subjects received University of Iowa Institutional Review Board approval (Protocol #230167). Mouse experimental protocols were reviewed and approved by the University of Iowa Institutional Animal Care and Use Committee (IACUC), in accordance with the National Institutes of Health guidelines.

Animal studies

BALB/c mice were obtained (Charles River Laboratories) and used at 6–8 weeks of age. Male and females mice of equal numbers were used for the experiments described unless specifically stated otherwise. Any observed sex specific effects on our data are discussed in the manuscript text. Mice were maintained in the University of Iowa Animal Care Unit under standard dark/light cycles, with controlled temperature and humidity. Mice had unlimited access to food and water, bedding is changed at least every seven days. Permission for these experiments was obtained from the University of Iowa Office of Animal Research and Institutional Animal Care and Use Committee (IACUC), as stated above. Mice are maintained and their welfare is ensured at all times by animal care staff under the direct supervision of a board certified veterinarian on-site. Any sick or injured mice are treated under the supervision of veterinary staff. Mice are immediately euthanized according to institutional protocols for animal welfare if any signs of unrecoverable illness or injury are present. Mice were randomly assigned to groups, with numbers sufficient to obtain statistical significance.

Human airway epithelial cells and cell line cultures

The University of Iowa *In Vitro* Models and Cell Culture Core cultured and maintained HAE as previously described.[79] Briefly, following enzymatic disassociation of trachea and bronchus epithelia, the cells were seeded onto collagen-coated, polycarbonate Transwell inserts (0 · 4 μm pore size; surface area = 0 · 33 cm^2; Corning Costar, Cambridge, MA). HAE were submerged in Ultroser G (USG)

media for 24 h (37°C and 5% CO_2) at which point the apical media is removed to allow cells to differentiate at an air-liquid interface. VeroE6 cells (ATCC CRL-1586) were grown in Dulbecco's Modified Eagle's Medium (DMEM) with 10% FBS. For experiments using primary HAE, cultures from 6 separate donors were obtained for the described experiments, with 1 sample from each donor exposed to each condition (e.g., vehicle, virus, and/or cytokines). Donor cells were from 5 males and 1 female, with 5 caucasian donors and 1 white-hispanic donor. Ages of donors varied between 16 and 64 years of age. We did not observe any sex related influence over the observed data.

SARS2-N501Y$_{MA30}$ virus

The SARS2-N501Y$_{MA30}$ was generated as previously described[47] and propagated in VeroE6 cells with input matching confirmed by genetic sequencing.

METHOD DETAILS

SARS-CoV-2 infection

Mice were anesthetized with ketamine/xylazine (87.5 mg/kg and 12.5 mg/kg) and inoculated intranasally with the indicated dosage of SARS2-N501Y$_{MA30}$ in 50 μL DMEM or DMEM alone. Mice were examined and weighed daily, and euthanized per institutional protocol if weight loss was >30%. At various time points, blood was collected from the submandibular vein, mice were euthanized, and indicated organs were collected. SARS-CoV-2 work was conducted in a Biosafety level 3 (BSL-3) laboratory.

Quantitative histopathology and immunohistochemistry

Lung tissues were fixed in 10% neutral buffered formalin (5–7 days), dehydrated through a progressive series of alcohol and xylene baths, paraffin-embedded, sectioned (~4 μm) and stained with hematoxylin and eosin (H&E) stain. Tissues were evaluated by a boarded veterinary pathologist and evaluated in a post-examination method of masking the pathologist to group assignment.[80] SARS-CoV-2 immunohistochemistry and scoring were performed as previously described[47] with minor modification in SARS-CoV-2 primary antibody (rabbit polyclonal anti-N-protein, Sino Bio 40143-T62, 1:4000 × 15 min). Briefly, edema and immunohistochemistry ordinal scores were based on distribution of each parameter in lung sections 0 – none, 1 - <25%, 2 - <50%, 3 < 75% and 4 - >75%.[81]

Antibodies and immunolocalization

Immunostaining was performed as described previously.[82] The following antibodies were used: SARS-CoV-2 N-protein (1:500, cat#40588-T62, RRID: AB_3064900, Sino Biological), goat anti-mouse C3 antibody (1:1000, cat#55463, MP Biomedicals), rat anti-mouse C9 (1:50, cat#HM1134-20UG), donkey anti-goat Alexa Fluor 488 (1:600, cat#A32814, Invitrogen), anti-alpha-tubulin (1:200, cat#5335S, Cell Signaling), anti-HopE1 (1:100, cat#sc-398703, Santa Cruz), anti-vWF (1:500, cat#AB7356, Millipore), and Alexa Fluor 546 phalloidin (1:600, cat#A22283, Invitrogen). Slides were mounted with Vectashield-DAPI (cat#H-1200, Vector Laboratories) and visualized with a Keyence BZ-X810 fluorescence microscope (Keyence Corporation of America).

Bioplex cytokine profiling

The levels of cytokines and chemokines in mouse serum and lung homogenates were determined using the Bio-Plex Multiplex Immunoassay System as described previously (Bioplex 200 machine, Biorad, Hercules, CA, USA).[83] Repeat freeze-thaw cycles were avoided to minimize protein degradation. The following cytokines and chemokines were measured using a Bioplex Express Kit according to the manufacturer's directions (Biorad, Hercules, CA, USA): GM-CSF, IFNγ, IL-6, IL-1β, RANTES, MCP-1, CXCL-1, CXCL-10.

Virus titers

Lungs were dissociated in 1X PBS using a Bead Mill homogenizer (Fisherbrand). Supernatants were serially diluted and added to VeroE6 cells, after 1 h incubation, incocula were replaced with 0.6% agarose containing 2%FBS in DMEM and after 4 days cells were fixed with 20% formaldehyde and stained with 1% crystal violet for plaque assay, with final titer quantified as PFU/mL.[47]

Western blot analysis

Mouse organ homogenates were combined with 1% NP40 and protease inhibitors per BSL-3 virus sterilization protocol and frozen. 20μg protein was loaded onto gels and run under reducing (C3, FB, and C9) or non-reducing (C4) conditions. Following electrophoresis and transfer to PVDF membranes, samples were blocked with 5% milk (2.5% milk for C4) and incubated with primary antibody anti-mouse C3 (1:500, cat#55463, MP Biomedicals), goat anti-human FB (1:500, cat#A311, Quidel), anti-mouse C9 (1:500, cat#HM1134, Hycult, or anti-mouse C4 (1:200, cat#ab11863, Abcam) overnight. The membrane was washed with Invitrogen Novex tricine SDS running buffer and incubated with HRP-conjugated or fluorescence tagged secondary for 1 h at room temperature, then developed using Supersignal West Pico Plus chemiluminescent kit (cat#34580, ThermoScientific). Protein signal was read using an Odyssey Imager. Membranes were stripped using Restore Western Stripping Buffer (cat#21059, ThermoScientific) and process repeated with anti-vinculin antibody (1:10,000, cat#700062, Invitrogen) as loading control. Densitometry analysis was performed

using ImageJ. Purified FB (cat#A135, Complement Technology), factor Bb (cat#A155, Complement Technology), and C3 (cat#A113, Complement Technology) were used for controls.

ELISA

Serum samples were collected by cheek vein puncture with blood passively collected in BD Microtainer tube. Samples are allowed to rest for 30 min on ice, and then centrifuged at 4°C for 10 min at 10,000 rcf. Serum was then collected and combined with protease inhibitor (cOmplete mini, EDTA free, #57621) at concentration of 20:1 and then placed on ice and inactivated under UV-light for 30 min per BSL-3 protocol for viral inactivation. All serum samples were then immediately transferred to a −80°C freezer for storage with only one freeze-thaw cycle before analysis. Serum from both infected and non-infected mice were subjected to sandwich ELISAs (Hycult Biotech, Uden, Ethiopia) to quantify activities of the AP and CP of the complement system. Additionally, we employed a separate ELISA (Aviva Systems Biology, San Diego, CA, USA) (Hycult, Uden, Ethiopia) to measure circulating levels of complement component 3 & 4 (C3 & C4). Data were analyzed using MyAssays software.

Cytokine stimulation of human airway epithelial cells

Cultures of HAE cells were propagated, plated, and matured as described above. Mature HAE cultures were treated with basolateral TNF-α (10 ng/mL) and IL-17 (20 ng/mL) daily and cells harvested at 5 h and 48 h post-cytokine stimulation. Cells were snap frozen and cell lysates were combined with Trizol and immediately stored at −80°C for preservation, with RNA sequencing performed as described below.

Mouse lung bulk RNA sequencing

RNA was extracted and purified from mouse lungs using the RNeasy plus mini-kit (QIAGEN). A cDNA library was prepared using the Illumina TruSeq stranded mRNA protocol. Library concentration and fragment size was measured using Qubit-HS and High-Sensitivity DNA Assay. The pooled library was sequenced on an Illumina NovaSeq 6000 SP Flowcell instrument for paired end reads. Library preparation, quality control, and sequencing were done by University of Iowa Genomics Facility.

Base calls were demultiplexed and converted to FASTQ format by the University of Iowa Genomics Facility. Fastq files were pseudo-aligned to the mouse reference genome.[84] Mapped raw reads were reported in transcripts per million by Kallisto. Downstream analysis was summarized as gene-level estimates using tximport v1·10 · 1 in Rv3·5.[85] Differential gene expression was performed using iDEP v0·92.[86] RNA-Seq data are available at GEO: GSE249304.

Human airway epithelial cell RNA sequencing

Bulk RNA-sequencing was performed in collaboration with the University of Iowa Genomics Division using the manufacturer's recommended protocols. Briefly, 500ng DNase I–treated total RNA was enriched for polyA-containing transcripts using beads coated with oligo(dT) primers. The enriched RNA pool was fragmented, converted to cDNA, and ligated to sequencing adaptors using the TruSeq stranded mRNA sample preparation kit (RS-122-2101, Illumina). The molar concentrations of the indexed libraries were measured using the 2100 Bioanalyzer (Agilent) and combined equally into pools for sequencing. The concentrations of the pools were measured with the Illumina Library Quantification Kit (KAPA Biosystems) and sequenced on the Illumina HiSeq 4000 genome sequencer using 75 bp paired-end SBS chemistry. Pseudoalignment of raw sequencing reads and quantification of transcript-level expression were obtained using Kallisto version 0 · 45·0 and human transcriptome reference GRCh38.[67] Gene counts were imported into R, and differential expression tests were performed using DESeq2 version 1 · 22·2.[68] Further, gene expression modeling in DESeq2 accounted for the experimental design, acknowledging and correcting for paired control and treated samples for each donor. Changes in complement related gene products were visualized as heatmaps generated using the Clustvis tool (https://biit.cs.ut.ee/clustvis/).[69] RNA-Seq data are available in the NCBI's GEO database (GEO: GSE176121 and GEO: GSE285099).

RNAscope

RNAscope was performed using the Advanced Cell Diagnostics protocol (ACD, Neward, CA). Formalin fixed and paraffin-embedded lung sections were deparaffinized in xylene and 100% ethanol, then dried. Target retrieval was performed using RNAscope Target Retrieval Reagents (ACD, cat#322000), following H_2O_2 then protease treatment using RNAscope H_2O_2 and Protease Plus (ACD, cat#322330). For *in-situ* hybridization slides were incubated with RNA probes for SARS-CoV-2 S (RNAscope Probe V-nCoV-2-S-C2) and C3 (RNAscope Probe Mm-C3-C3), then mounted with DAPI Mounting Media (ACD).

QUANTIFICATION AND STATISTICAL ANALYSIS

Statistics were performed using Graph Pad Prism 10 Software. Tests included Kaplan-Meier, unpaired or paired 2-tailed Student's t test for comparing 2 groups, 1-way ANOVA with multiple comparison test for comparing more than 2 groups. Tests used are described in figure legend. P-value of <0.05 was considered significant (*, p values $\leq$0.05, **, p values $\leq$0.01, ***, p values $\leq$ 0.001, ****, p values $\leq$0.0001).